0021-972X/03/$15.00/0
*Printed in U.S.A.*

The Journal of Clinical Endocrinology & Metabolism 88(11):5473–5477

doi: 10.1210/jc.2002-021350

# Ghrelin Concentration in Cord and Neonatal Blood: Relation to Fetal Growth and Energy Balance

SEIKO KITAMURA, ICHIRO YOKOTA, HIROSHI HOSODA, YUMIKO KOTANI, JUNKO MATSUDA, ETSUO NAITO, MICHINORI ITO, KENJI KANGAWA, AND YASUHIRO KURODA

*Department of Pediatrics, University of Tokushima School of Medicine (S.K., I.Y., Y.Ko., J.M., E.N., M.I., Y.Ku.), Tokushima 770-8503, Japan; and Department of Biochemistry, National Cardiovascular Center Research Institute (H.H., K.K.), Osaka 565-8565, Japan*

**To investigate the relationship between ghrelin and both fetal and neonatal growth parameters and energy balance, we measured plasma ghrelin concentrations in 54 cord blood samples (male, n = 34; female, n = 20; gestational age, 37.0–41.6 wk; birth weight, 2206–4326 g) and 47 neonatal blood samples (male, n = 27; female, n = 20; postnatal d 3–8). The plasma ghrelin concentrations in cord blood ranged from 110.6–446.1 pmol/liter (median, 206.7 pmol/liter), which were equal to or higher than those in normal weight adults. These values were inversely correlated with birth weight (r = −0.40; $P = 0.002$), birth length (r = −0.36; $P = 0.007$), placental weight (r = −0.35; $P = 0.01$), and IGF-I concentration (r = −0.49; $P = 0.0002$), but were not significantly correlated with the GH concentration (r = 0.22; $P = 0.12$). The ghrelin concentrations in small for gestational age newborn were significantly higher than those in appropriate for gestational age newborns ($P = 0.0008$). The ghrelin concentrations in the vein were significantly higher than those in the artery in 8 cord blood samples ($P = 0.01$), which suggests that the placenta is an important source of fetal ghrelin. In neonates, the ghrelin concentrations ranged from 133.0–481.7 pmol/liter (median, 268.3 pmol/liter), which were significantly higher than those in cord blood ($P < 0.0001$). These results suggest that ghrelin may contribute to fetal and neonatal growth. (*J Clin Endocrinol Metab* 88: 5473–5477, 2003)**

GHRELIN IS AN endogenous ligand for the GH secretagogue receptor that stimulates the release of GH (1, 2). In addition, ghrelin positively regulates the energy balance as an antagonist of leptin through hypothalamic nuclei (3, 4). These actions seem to be especially important during the growth stage in humans. In adults, the major source of circulating ghrelin in the blood comes from the neuroendocrine cells in the fundus of the stomach (5, 6), and the level of ghrelin rises during fasting and falls to a nadir after eating (7). Significantly decreased ghrelin levels have been observed in obese individuals (8, 9).

We previously reported changes in the leptin concentration during the fetal and neonatal periods (10–12). A relatively high level of leptin at birth and the expression of leptin in the placenta suggested that leptin may play a role during the perinatal period (10–13). Interestingly, ghrelin has also been reported to be expressed in the placenta (14). Therefore, it is important to examine changes in the ghrelin concentration during the fetal and neonatal periods to evaluate the relation between ghrelin and both the growth of the fetus and neonate and the regulation of feto-maternal and neonatal energy balance.

In the present study we measured ghrelin concentrations in cord and neonatal blood using a specific RIA system we developed (15), and examined its relationship to other growth-related hormones and clinical characteristics of the fetus and neonate.

Abbreviations: AGA, Appropriate for gestational age; IRI, immunoreactive insulin; LGA, large for gestational age; SGA, small for gestational age.

## Subjects and Methods

### *Subjects*

Venous cord blood samples were obtained from 54 full-term newborns (34 males and 20 females; gestational age, 37.0–41.6 wk; birth weight, 2206–4326 g; birth length, 44.0–54.5 cm). Their characteristics are shown in Table 1. Forty-four of the newborns were classified as appropriate for gestational age (AGA), 7 were small for gestational age (SGA), and 3 were large for gestational age (LGA). AGA was defined as a newborn whose birth weight was from −1.5 to +1.5 SD of the mean birth weight in each gestational age. SGA was defined as below −1.5 SD, and LGA was defined as over +1.5 SD. The mean birth weight and SD were calculated according to the Japanese population fetal growth curve published in 1994 by a study group of the Japanese Ministry of Health and Welfare. To estimate the source of ghrelin in the fetal circulation, both arterial and venous cord blood samples were collected from another 8 full-term newborns. Blood samples for ghrelin assay were collected in chilled tubes containing EDTA·2Na (1 mg/ml) and aprotinin (500 U/ml), and plasma was separated at 4 C immediately after birth. Serum was simultaneously separated for other hormone assays. Neonatal samples were obtained from 47 full-term healthy neonates (27 males and 20 females; postnatal d 3–8), whose characteristics are shown at Table 2. In 27 of these neonates, cord blood had already been collected, and the change in the ghrelin concentration between cord and neonatal blood was compared in this group. Each sample was collected at 0900 h, and plasma was separated immediately.

Plasma and serum samples were kept frozen at −80 C until analysis. All of the newborns and neonates were healthy, and their mothers had had no remarkable complications during pregnancy. The study protocol was approved by the ethical committee of University of Tokushima School of Medicine, and all parents of the newborns gave their written informed consent before enrollment.

### *Ghrelin and other hormone assays*

Plasma ghrelin concentration was determined by RIA using polyclonal antibodies raised against the carboxyl-terminal fragment ghrelin-[13–28] (15). The value determined by this RIA system gives the total concentration of ghrelin. Serum GH and IGF-I were determined using

**TABLE 1.** Characteristics of the fetus and plasma ghrelin concentration in cord blood

| | Total (n = 54) | Male (n = 34) | Female (n = 20) |
|---|---|---|---|
| Gestational wk | 39.4 (37.0–41.6) | 39.5 (37.0–41.4) | 39.3 (37.0–41.6) |
| Birth body weight (g) | 2994 (2206–4326) | 3008 (2206–3778) | 2884 (2318–4326) |
| Birth body length (cm) | 48.5 (44.0–54.5) | 48.5 (44.0–52.5) | 48.3 (46.0–54.5) |
| Kaup index (g/cm$^2$ × 10) | 12.6 (10.6–15.3) | 12.8 (10.6–15.3) | 12.5 (11.0–15.2) |
| Birth weight/birth length (g/cm) | 60.9 (49.0–79.4) | 61.5 (49.0–74.1) | 60.6 (50.4–79.4) |
| Placental weight (g) | 532 (322–804) | 514 (325–804) | 562 (322–783) |
| Plasma ghrelin (pmol/liter) | 206.7 (110.6–446.1) | 207.8 (110.6–404.2) | 201.1 (119.2–446.1) |

Values are medians, with the range in *parentheses*.

**TABLE 2.** Characteristics of the neonate and plasma ghrelin concentration in neonatal blood

| | Total (n = 47) | Male (n = 27) | Female (n = 20) |
|---|---|---|---|
| Days after birth | 5.0 (3.0–8.0) | 5.0 (3.0–8.0) | 5.0 (3.0–6.0) |
| Gestational wk | 39.3 (37.0–41.4) | 39.4 (37.0–41.4) | 39.1 (37.0–40.6) |
| Birth body weight (g) | 3030 (2324–4082) | 3030 (2620–3994) | 2961 (2324–4082) |
| Body weight (g) | 2870 (2246–3816) | 2966 (2530–3650) | 2758 (2246–3816) |
| Body length (cm) | 48.9 (44.0–52.0) | 49.0 (44.0–51.5) | 48.6 (45.0–52.0) |
| Mean calorie intake (kcal/kg·d) | 66.5 (35.3–105.8) | 57.1 (41.0–105.8) | 72.4 (35.3–97.0) |
| Body weight loss for 5 d (%) | 4.9 (0.5–24.3) | 3.9 (0.5–24.3) | 6.4 (1.7–9.7) |
| Body weight gain for 1 month (g/d) | 46.5 (12.3–69.4) | 47.7 (12.3–69.4) | 45.7 (30.4–57.9) |
| Plasma ghrelin (pmol/liter) | 268.3 (133.0–481.7) | 272.0 (133.0–421.0) | 265.0 (172.3–481.7) |

Values are medians, with the range in *parentheses*.

immunoradiometric assay kits (Daiichi Radioisotope Laboratories, Tokyo, Japan). Serum IGF-II was determined using an ELISA kit (Diagnostic Systems Laboratories, Inc., Sinsheim, Germany). Serum immunoreactive insulin (IRI) was determined using an immunoradiometric assay kit (Eiken Chemical, Tokyo, Japan). Serum IGF-binding protein-3 was determined using an RIA kit (Cosmic Corp., Tokyo, Japan). Serum leptin was determined using an RIA kit (Linco Research, Inc., St. Charles, MO).

### *Statistical analysis*

All quantitative data are presented as the median and range. Pearson's correlations were used to examine relationships among clinical growth-related parameters and hormone levels. Differences between groups were evaluated by Mann-Whitney *U* test or Wilcoxon's signed rank test. Significance was considered to be $P < 0.05$. The analysis was conducted with StatView software (version 5.0 for Windows, SAS Institute, Inc., Cary, NC) or SPSS software (version 11.0J for Windows, SPSS. Inc., Chicago, IL).

## Results

In 54 cord blood samples, plasma ghrelin concentrations ranged from 110.6–446.1 pmol/liter (median, 206.7 pmol/liter). Ghrelin concentrations were inversely correlated with birth weight ($r = -0.40$; $P = 0.002$), birth length ($r = -0.36$; $P = 0.007$), placental weight ($r = -0.35$; $P = 0.01$), birth weight/birth length ratio ($r = -0.38$; $P = 0.004$), Kaup index ($r = -0.28$; $P = 0.04$), IGF-I concentration ($r = -0.49$; $P = 0.0002$), and IGF-binding protein-3 concentration ($r = -0.30$; $P = 0.03$). Ghrelin concentrations in SGA newborn were significantly higher than those in AGA and LGA newborns ($P = 0.0008$ and $P = 0.02$, respectively; Figs. 1 and 2). No significant correlation was observed between ghrelin and GH concentrations ($r = 0.22$; $P = 0.12$; Fig. 2 and Tables 1 and 3).

As some anthropometrical parameters and IGF-I concentrations were inversely correlated with ghrelin concentrations, we performed some partial correlation analyses to determine which factor was predominantly correlated with them. The partial correlation analysis calculates a correlation between two variables while controlling for the effect of other additional variables. The partial correlation between ghrelin and IGF-I, while controlling for birth weight, birth length, or placental weight, was still significant ($r = -0.43$, $-0.47$, and

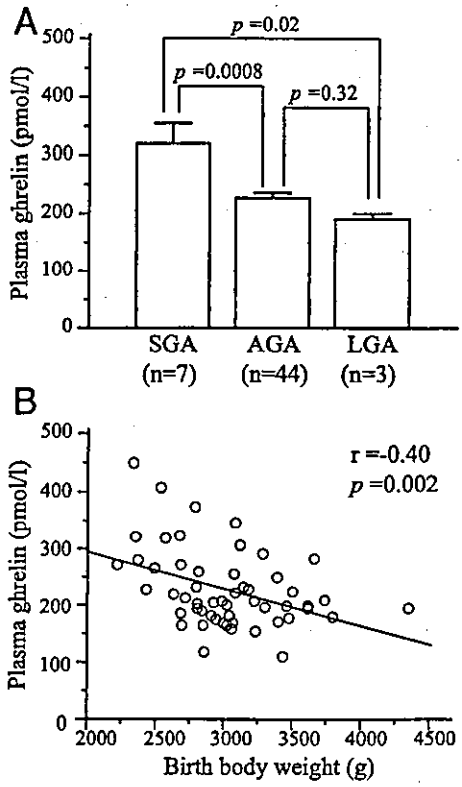


FIG. 1. A, Comparison of plasma ghrelin concentrations in SGA, AGA, and LGA newborns (mean ± SEM). Ghrelin concentrations in SGA newborns were significantly higher than those in AGA and LGA newborns. B, Inverse correlation between plasma ghrelin concentration and birth weight for the subjects in A. The *solid line* represents the regression line.

−0.39; $P = 0.002$, 0.001, and 0.006, respectively). On the other hand, the partial correlation between ghrelin and birth weight, birth length, or placental weight, while controlling for IGF-I, showed diminished statistical significance (r = −0.26, −0.28, and −0.19; $P = 0.07$, 0.05, and 0.20, respectively). These results suggest that IGF-I is a predominant factor that is correlated with the ghrelin concentration. The partial correlation between ghrelin and GH while controlling for each anthropometrical parameter or IGF-I confirmed the absence of a significant correlation between GH and ghrelin concentrations.

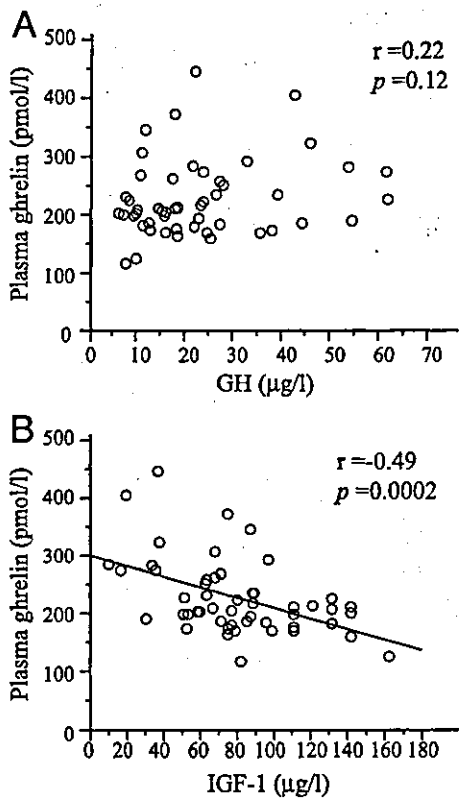


FIG. 2. A, Correlation between the ghrelin and GH concentrations in cord blood. No significant correlation was observed. B, A significant inverse correlation was seen between ghrelin and IGF-I concentrations in cord blood. The *solid line* represents the regression line.

In the eight newborns whose cord blood samples were collected from both the artery and vein, plasma ghrelin concentrations in the vein (median, 304.9 pmol/liter; range, 218.7–403.8 pmol/liter) were significantly higher than those in the artery (median, 287.5 pmol/liter; range, 181.9–392.4 pmol/liter; $P = 0.01$; Fig. 3).

In neonates, the plasma ghrelin concentrations ranged from 133.0–481.7 pmol/liter (median, 268.3 pmol/liter), which were significantly higher than those in cord blood ($P < 0.0001$). The sequential analysis of ghrelin concentrations after birth in 27 newborns confirmed that the ghrelin concentrations significantly increased during the early neonatal period ($P < 0.0001$; Fig. 4). The ghrelin concentrations in neonates did not significantly correlate with percentage body weight loss from birth to the sampling day (r = −0.13; $P = 0.37$), calorie intake per body weight on the sampling day (r = 0.04; $P = 0.80$), or the mean daily body weight gain during the first month of life (r = 0.23; $P = 0.13$; Table 4). No significant gender difference in ghrelin concentration was observed in either cord or neonatal blood (Tables 1 and 2).

## Discussion

Our results showed that ghrelin is present in cord and neonatal blood at concentrations 1.5- to 2-fold higher than those found in normal weight adult (6, 9). The existence of ghrelin in cord blood is consistent with previous observations, although the use of nonextracted plasma is different compared with our study (16).

In adults, the plasma ghrelin concentration is mainly determined by the energy balance. Patients with anorexia nervosa and cachexia show elevated levels of ghrelin (6, 17), whereas obese subjects have reduced levels (8, 9). Thus, it is interesting that ghrelin concentrations were inversely correlated with several growth-related anthropometric parameters and the IGF-I concentration in the fetus. This result

**TABLE 3A.** Correlation coefficients between cord blood levels and size at birth

| | Ghrelin | GH | IGF-I | IGF-II | IGFBP-3 | Leptin | Insulin |
|---|---|---|---|---|---|---|---|
| Birth weight | −0.40[a] | −0.38[b] | 0.30[b] | −0.05 | 0.23 | 0.53[c] | 0.34[b] |
| Birth length | −0.36[b] | −0.41[a] | 0.18 | −0.23 | 0.15 | 0.25 | 0.24 |
| Kaup index | −0.28[b] | −0.19 | 0.30[b] | 0.19 | 0.23 | 0.54[c] | 0.27 |
| Body weight/body length | −0.38[a] | −0.32[b] | 0.32[b] | 0.05 | 0.25 | 0.56[c] | 0.33[b] |
| Placental weight | −0.35[b] | −0.21 | 0.33[b] | −0.23 | 0.12 | 0.27 | 0.08 |

**TABLE 3B.** Correlation coefficients between cord blood levels

| | Median (range) | Ghrelin | GH | IGF-I | IGF-II | IGFBP-3 | Leptin |
|---|---|---|---|---|---|---|---|
| GH (μg/liter) | 17.8 (5.7–61.0) | 0.22 | | | | | |
| IGF-I (μg/liter) | 77 (12–160) | −0.49[d] | −0.47[d] | | | | |
| IGF-II (μg/liter) | 310 (181–481) | −0.13 | 0.08 | 0.02 | | | |
| IGFBP-3 (mg/liter) | 0.76 (0.45–1.28) | −0.30[e] | −0.40[f] | 0.72[d] | 0.22 | | |
| Leptin (μg/liter) | 3.5 (0.8–13.8) | −0.12 | −0.06 | 0.14 | 0.30[e] | 0.28[e] | |
| Insulin (pmol/liter) | 11.4 (6.0–100.2) | −0.17 | −0.26 | 0.25 | −0.15 | 0.20 | 0.01 |

IGFBP-3, IGF binding protein-3.
[a] $P < 0.005$.
[b] $P < 0.05$.
[c] $P < 0.0005$.
[d] $P < 0.0005$.
[e] $P < 0.05$.
[f] $P < 0.005$.

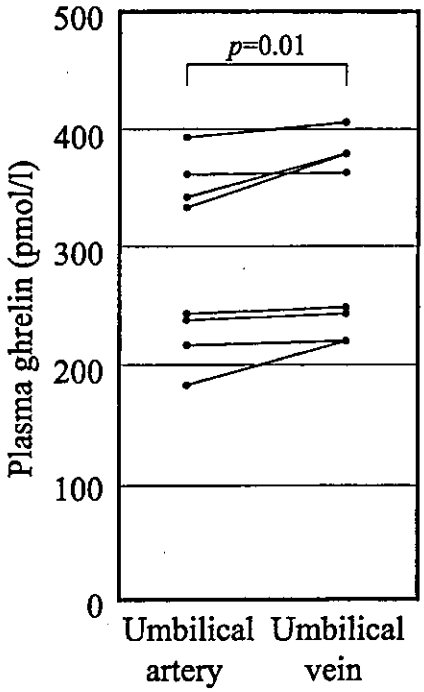


FIG. 3. Comparison of plasma ghrelin concentrations in arterial and venous cord blood. The plasma ghrelin concentrations in arterial and venous cord blood were compared in eight full-term newborns. Each *bar* links the arterial and venous ghrelin concentrations in each newborn. The plasma ghrelin concentrations in the vein were significantly higher than those in the artery ($P = 0.01$).

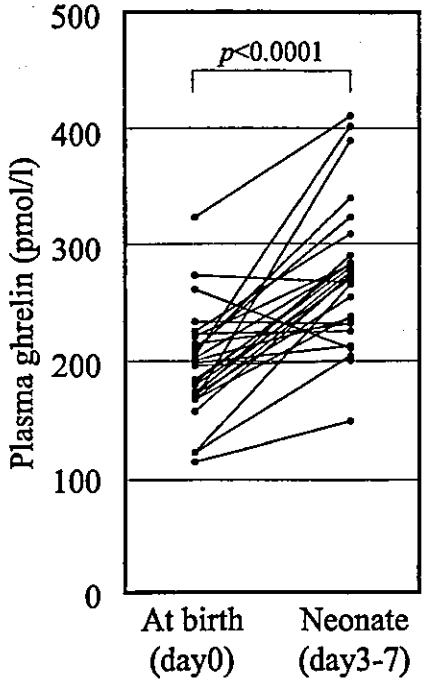


FIG. 4. Change in plasma ghrelin concentration after birth. The plasma ghrelin concentrations at birth (cord blood) and during the early neonatal period (postnatal d 3–7) were compared in 27 newborns (male, n = 18; female, n = 9). Each *bar* represents the change in the ghrelin concentration in each newborn. Ghrelin concentrations during the early neonatal period were significantly higher than those in cord blood ($P < 0.0001$).

**TABLE 4.** Correlation coefficients between neonatal ghrelin levels and energy balance

| | Ghrelin (*P*) |
|---|---|
| Birth weight | −0.21 (0.16) |
| Body weight | −0.17 (0.26) |
| Body length | −0.22 (0.14) |
| Kaup index | −0.10 (0.49) |
| Mean calorie intake[a] | 0.04 (0.80) |
| Body weight loss[b] | −0.13 (0.37) |
| Body weight gain[c] | 0.23 (0.13) |

[a] Calorie intake per body weight on sampling day (kilocalories per kilogram).
[b] Percentage body weight loss from birth to sampling day (percentage).
[c] Mean daily body weight gain during first month of life (grams per day).

suggests that the ghrelin concentration might be mainly regulated in a fetal growth-related manner *in utero*, as if its role was to accelerate fetal growth. In an experimental study, a significant level of GH secretagogue receptor expression was observed in the fetal rat hypothalamus, pituitary, and brainstem (18). However, fetal GH may not contribute to fetal growth itself to a large extent, as patients with Pit-1 gene or GH-1 gene deficiency, which are congenital disorders of pituitary GH synthesis, show nearly normal fetal growth. Fetal growth essentially depends on the energy transport from the mother. A positive correlation between size at birth and cord blood IGF-I concentration has been reported (19, 20). Considering that the ghrelin concentration correlated not with GH but with the IGF-I concentration, and the remarkable elevation of the ghrelin concentration in SGA newborns, negative feedback regulation between fetal growth and the ghrelin concentration may not originate in the fetal GH axis, but, rather, in feto-maternal energy transport, which would affect fetal growth and the IGF-I level.

In the rat, ghrelin mRNA is expressed at a very low level in the fetal stomach (21, 22), whereas significant expression is observed in the placenta (14). In humans, ghrelin mRNA is also expressed in the placenta (14). Therefore, it is possible that some of the ghrelin in the fetal circulation might originate from the placenta, like leptin, and regulate feto-maternal energy transport locally, as ghrelin concentrations in the umbilical vein were significantly higher than those in the artery. In addition, immunohistochemical studies of the human fetus showed that ghrelin-immunoreactive cells were fairly well represented in the stomach, duodenum, pancreas, and lung from wk 10 of gestation (23, 24). The contributions of these peripheral organs may also be taken into consideration.

In our previous study the leptin concentration rapidly decreased after birth and remained at a low level during the early neonatal period (11). In contrast, plasma ghrelin concentrations at approximately 5 d after birth were significantly higher than those in cord blood. After birth, the energy supply through the placenta is interrupted, and a newborn needs to start taking milk for growth. Thus, in contrast to leptin, which reduces energy intake, it is reasonable for the ghrelin concentration in neonates to increase to stimulate appetite and give a positive energy balance. However, in rat stomach, the expression of ghrelin mRNA in neonates is lower than

that in adults (21, 22). The origin of the high concentration of ghrelin in neonates may need further investigation, with regard not only to its synthesis and secretion, but also to its degradation and clearance during the neonatal period.

In summary, this study demonstrates the existence of ghrelin in fetal and neonatal blood at rather high concentrations, an inverse correlation between the cord blood ghrelin concentrations and fetal growth-related parameters, and a significant elevation of the ghrelin concentration during the early neonatal period. Further study of ghrelin concentrations in fetuses and neonates with pathological status, such as premature delivery or severe intrauterine growth retardation, may provide useful information about regulation of the ghrelin concentration and its role during the fetal and neonatal periods.

## Acknowledgments

We thank Dr. K. Maeda and Prof. M. Irahara (Department of Obstetrics and Gynecology, University of Tokushima School of Medicine) for their support with the sample collection.

Received August 22, 2002. Accepted July 31, 2003.

Address all correspondence and requests for reprints to: Ichiro Yokota, M.D., Department of Pediatrics, University of Tokushima School of Medicine, 3-Kuramoto cho, Tokushima 770-8503, Japan. E-mail: yichiro@clin.med.tokushima-u.ac.jp.

This work was supported in part by a grant from the Foundation for Growth Science (Tokyo, Japan).

## References

1. **Kojima M, Hosoda H, Date Y, Nakazato M, Matsuo H, Kangawa K** 1999 Ghrelin is a growth-hormone-releasing acylated peptide from stomach. Nature 402:656–660
2. **Takaya K, Ariyasu H, Kanamoto N, Iwakura H, Yoshimoto A, Harada M, Mori K, Komatsu Y, Usui T, Shimatsu A, Ogawa Y, Hosoda K, Akamizu T, Kojima M, Kangawa K, Nakao K** 2000 Ghrelin strongly stimulates growth hormone release in humans. J Clin Endocrinol Metab 85:4908–4911
3. **Nakazato M, Murakami N, Date Y, Kojima M, Matsuo H, Kangawa K, Matsukura S** 2001 A role for ghrelin in the central regulation of feeding. Nature 409:194–198
4. **Kamegai J, Tamura H, Shimizu T, Ishii S, Sugihara H, Wakabayashi I** 2000 Central effect of ghrelin, an endogenous growth hormone secretagogue, on hypothalamic peptide gene expression. Endocrinology 141:4797–4800
5. **Date Y, Kojima M, Hosoda H, Sawaguchi A, Mondal MS, Suganuma T, Matsukura S, Kangawa K, Nakazato M** 2000 Ghrelin, a novel growth hormone-releasing acylated peptide, is synthesized in a distinct endocrine cell type in the gastrointestinal tracts of rats and humans. Endocrinology 141: 4255–4261
6. **Ariyasu H, Takaya K, Tagami T, Ogawa Y, Hosoda K, Akamizu T, Suda M, Koh T, Natsui K, Toyooka S, Shirakami G, Usui T, Shimatsu A, Doi K, Hosoda H, Kojima M, Kangawa K, Nakao K** 2001 Stomach is a major source of circulating ghrelin, and feeding state determines plasma ghrelin-like immunoreactivity levels in humans. J Clin Endocrinol Metab 86:4753–4758
7. **Cummings DE, Purnell JQ, Frayo RS, Schmidova K, Wisse BE, Weigle DS** 2001 A preprandial rise in plasma ghrelin levels suggests a role in meal initiation in humans. Diabetes 50:1714–1719
8. **Tschop M, Weyer C, Tataranni PA, Devanarayan V, Ravussin E, Heiman ML** 2001 Circulating ghrelin levels are decreased in human obesity. Diabetes 50: 707–709
9. **Shiiya T, Nakazato M, Mizuta M, Date Y, Mondal MS, Tanaka M, Nozoe S, Hosoda H, Kangawa K, Matsukura S** 2002 Plasma ghrelin levels in lean and obese humans and the effect of glucose on ghrelin secretion. J Clin Endocrinol Metab 87:240–244
10. **Matsuda J, Yokota I, Iida M, Murakami T, Naito E, Ito M, Shima K, Kuroda Y** 1997 Serum leptin concentration in cord blood: relationship to birth weight and gender. J Clin Endocrinol Metab 82:1642–1644
11. **Matsuda J, Yokota I, Iida M, Murakami T, Yamada M, Saijo T, Naito E, Ito M, Shima K, Kuroda Y** 1999 Dynamic changes in serum leptin concentrations during the fetal and neonatal periods. Pediatr Res 45:71–75
12. **Matsuda J, Yokota I, Tsuruo Y, Murakami T, Ishimura K, Shima K, Kuroda Y** 1999 Developmental changes in long-form leptin receptor expression and localization in rat brain. Endocrinology 140:5233–5238
13. **Masuzaki H, Ogawa Y, Sagawa N, Hosoda K, Matsumoto T, Mise H, Nishimura H, Yoshimasa Y, Tanaka I, Mori T, Nakao K** 1997 Nonadipose tissue production of leptin: leptin as a novel placenta-derived hormone in humans. Nat Med 3:1029–1033
14. **Gualillo O, Caminos J, Blanco M, Garcia-Caballero T, Kojima M, Kangawa K, Dieguez C, Casanueva F** 2001 Ghrelin, a novel placental-derived hormone. Endocrinology 142:788–794
15. **Hosoda H, Kojima M, Matsuo H, Kangawa K** 2000 Ghrelin and des-acyl ghrelin: two major forms of rat ghrelin peptide in gastrointestinal tissue. Biochem Biophys Res Commun 279:909–913
16. **Chanoine JP, Yeung LP, Wong AC, Birmingham CL** 2002 Immunoreactive ghrelin in human cord blood: relation to anthropometry, leptin, and growth hormone. J Pediatr Gastroenterol Nutr 35:282–286
17. **Nagaya N, Uematsu M, Kojima M, Date Y, Nakazato M, Okumura H, Hosoda H, Shimizu W, Yamagishi M, Oya H, Koh H, Yutani C, Kangawa K** 2001 Elevated circulating level of ghrelin in cachexia associated with chronic heart failure: relationships between ghrelin and anabolic/catabolic factors. Circulation 104:2034–2038
18. **Katayama M, Nogami H, Nishiyama J, Kawase T, Kawamura K** 2000 Developmentally and regionally regulated expression of growth hormone secretagogue receptor mRNA in rat brain and pituitary gland. Neuroendocrinology 72:333–340
19. **Klauwer D, Blum WF, Hanitsch S, Rascher W, Lee PD, Kiess W** 1997 IGF-I, IGF-II, free IGF-I and IGFBP-1, -2 and -3 levels in venous cord blood: relationship to birthweight, length and gestational age in healthy newborns. Acta Paediatr 86:826–833
20. **Ong K, Kratzsch J, Kiess W, Costello M, Scott C, Dunger D** 2000 Size at birth and cord blood levels of insulin, insulin-like growth factor I (IGF-I), IGF-II, IGF-binding protein-1 (IGFBP-1), IGFBP-3, and the soluble IGF-II/mannose-6-phosphate receptor in term human infants. The ALSPAC Study Team. Avon Longitudinal Study of Pregnancy and Childhood. J Clin Endocrinol Metab 85:4266–4269
21. **Lee HM, Wang G, Englander EW, Kojima M, Greeley GH Jr** 2002 Ghrelin, a new gastrointestinal endocrine peptide that stimulates insulin secretion: enteric distribution, ontogeny, influence of endocrine, and dietary manipulations. Endocrinology 143:185–190
22. **Hayashida T, Nakahara K, Mondal MS, Date Y, Nakazato M, Kojima M, Kangawa K, Murakami N** 2002 Ghrelin in neonatal rats: distribution in stomach and its possible role. J Endocrinol 173:239–245
23. **Rindi G, Necchi V, Savio A, Torsello A, Zoli M, Locatelli V, Raimondo F, Cocchi D, Solcia E** 2002 Characterization of gastric ghrelin cells in man and other mammals: studies in adult and fetal tissues. Histochem Cell Biol 117: 511–519
24. **Volante M, Fulcheri E, Allia E, Cerrato M, Pucci A, Papotti M** 2002 Ghrelin expression in fetal, infant, and adult human lung. J Histochem Cytochem 50:1013–1021

**Journal of Pathology**
*J Pathol* 2003; **201**: 149–159.
Published online 30 May 2003 in Wiley InterScience (www.interscience.wiley.com). **DOI**: 10.1002/path.1414

**Original Paper**

# Platelet-derived growth factor and its receptors are related to the progression of human muscular dystrophy: an immunohistochemical study

Yajuan Zhao,[1,2] Kazuhiro Haginoya,[1]* Guilian Sun,[1] Hongmei Dai,[1] Akira Onuma[3] and Kazuie Iinuma[1]
[1]*Department of Pediatrics, Tohoku University School of Medicine, Sendai 980-8574, Japan*
[2]*Department of Pediatrics, Second Clinical College of China Medical University, Shenyang, China*
[3]*Department of Pediatrics, Takutou Rehabilitation Center for Disabled Children, Sendai, Japan*

*Correspondence to:
*Kazuhiro Haginoya, MD, Department of Pediatrics, Tohoku University School of Medicine, 1-1 Seiryomachi, Aobaku, Sendai 980-8574, Japan.*
*E-mail: khaginoya@ped.med.tohoku.ac.jp*

## Abstract

**This study has examined the immunological localization of platelet-derived growth factor (PDGF)-A, PDGF-B, and PDGF receptor (PDGFR) alpha and beta to clarify their role in the progression of muscular dystrophy. Biopsied frozen muscles from patients with Duchenne muscular dystrophy (DMD), Becker muscular dystrophy (BMD), and congenital muscular dystrophy (CMD) were analysed immunohistochemically using antibodies raised against PDGF-A, PDGF-B, and PDGFR alpha and beta. Muscles from two dystrophic mouse models (*dy* and *mdx* mice) were also immunostained with antibodies raised against PDGFR alpha and beta. In normal human control muscle, neuromuscular junctions and vessels were positively stained with antibodies against PDGF-A, PDGF-B, PDGFR alpha and PDGFR beta. In human dystrophic muscles, PDGF-A, PDGF-B, PDGFR alpha and PDGFR beta were strongly immunolocalized in regenerating muscle fibres and infiltrating macrophages. PDGFR alpha was also immunolocalized to the muscle fibre sarcolemma and necrotic fibres. The most significant finding in this study was a remarkable overexpression of PDGFR beta and, to a lesser extent, PDGFR alpha in the endomysium of DMD and CMD muscles. PDGFR was also overexpressed in the interstitium of muscles from dystrophic mice, particularly *dy* mice. Double immunolabelling revealed that activated interstitial fibroblasts were clearly positive for PDGFR alpha and beta. However, DMD and CMD muscles with advanced fibrosis showed very poor reactivity against PDGF and PDGFR. Those findings were confirmed by immunoblotting with PDGFR beta. These findings indicate that PDGF and its receptors are significantly involved in the active stage of tissue destruction and are associated with the initiation or promotion of muscle fibrosis. They also have roles in muscle fibre regeneration and signalling at neuromuscular junctions in both normal and diseased muscle. Copyright © 2003 John Wiley & Sons, Ltd.**

Received: 12 August 2002
Revised: 7 January 2003
Accepted: 26 March 2003

**Keywords:** **platelet-derived growth factor; platelet-derived growth factor receptor alpha; platelet-derived growth factor receptor beta; muscular dystrophy; fibrosis; *mdx* mice; *dy* mice**

## Introduction

The progression of muscular weakness in patients suffering from Duchenne muscular dystrophy (DMD) and congenital muscular dystrophy (CMD) correlates directly with the progressive loss of myofibres, which is accompanied by connective tissue and adipose tissue replacement. The mechanism of histological progression remains unclear. Previous studies suggest that there is a progressive loss of regenerating capacity in muscle fibres [1]. Interstitial fibrosis may be attributed to a loss of regenerating capacity in satellite cells, which is caused by a reduced blood supply to individual muscle fibres [2,3]. Alternatively, Melone *et al* recently proposed that growth factors released locally by diseased muscle tissue may reduce the regenerating capacity of satellite cells [4,5]. Recent studies also suggest that growth factors such as transforming growth factor beta 1 (TGF$\beta$1) and basic fibroblast growth factor (bFGF) have important roles in disease progression [6–10].

Platelet-derived growth factor (PDGF) consists of two disulphide-linked peptide chains, A and B, and occurs naturally in three isoforms, PDGF-AA, PDGF-AB, and PDGF-BB [11]. PDGF is a growth stimulant and chemoattractant, principally for mesenchymal connective tissue-forming cells [11,12]. By binding to specific high-affinity cell surface receptors, PDGF induces cell proliferation and a number of other critical processes. There are two PDGF receptor subunits; the alpha subunit (PDGFR alpha) binds both the PDGF-A and the PDGF-B chains, while the beta subunit (PDGFR beta) binds only the PDGF-B chain [13]. There have been some reports of PDGF and PDGFR

expression in muscle tissue. PDGF-A chain mRNA and PDGFR beta mRNA are expressed in rat L6 cultured myoblasts [14,15] and PDGFR beta immunoreactivity has been reported in regenerating muscle fibres of dystrophin-deficient *mdx* mice [16]. L6 myoblasts bind the PDGF-BB isoform, but not the PDGF-AA isoform, and the addition of PDGF-BB to culture media results in myoblast proliferation and the inhibition of myoblast differentiation [17]. These results suggest that the BB isoform of PDGF has a significant effect on skeletal muscle regeneration.

There have been no studies of the functional role of PDGF and its receptors in diseased human muscle. This prompted us to examine the immunolocalization of PDGF-A, PDGF-B, PDGFR alpha, and PDGFR beta in biopsied muscle from patients with various types of muscular dystrophy to clarify their role in disease progression. In addition, we compared PDGFR alpha and beta expression in muscles from *dy* and *mdx* mice to confirm the results from human muscles.

## Materials and methods

We studied diagnostic muscle biopsies from 32 patients, aged 8 months to 18 years. Written informed consent to use these specimens for research was obtained from all of the patients' families. Of the biopsies studied, eight had a diagnosis of DMD, nine had congenital muscular dystrophy (CMD) [six with Fukuyama-type CMD (FCMD) and three with merosin-positive CMD], five had Becker muscular dystrophy (BMD), and ten were normal. Diagnosis was based on clinical, laboratory, muscle biopsy histochemistry, and dystrophin and merosin immunohistochemistry. A clinical summary of the patients is given in Table 1. Transverse sections (10 μm) of fresh-frozen muscle biopsies were used for immunohistochemical staining. For the detection of PDGF-A, PDGF-B, PDGFR alpha, and PDGFR beta, affinity-purified rabbit antisera were raised against the following: (1) a synthetic peptide mapping to the carboxy-terminal of human PDGF-A (sc-128; Santa Cruz Biotechnology; dilution 1 : 400; 0.5 μg/ml); (2) a synthetic peptide (amino acid sequence 136–190) mapping to the carboxy-terminal of mature human PDGF-B (sc-7878; Santa Cruz Biotechnology; dilution 1 : 400; 0.5 μg/ml); (3) a synthetic peptide mapping to the carboxy-terminal of human PDGFR alpha (sc-338; Santa Cruz Biotechnology; dilution 1 : 400; 0.5 μg/ml); and (4) a synthetic peptide mapping to the carboxy-terminal of human PDGFR beta (sc-339; Santa Cruz Biotechnology; dilution 1 : 400; 0.5 μg/ml).

Indirect immunoperoxidase (ABC) (Vectastain ABC kit; Vector, Burlingame, CA, USA) and immunofluorescence methods were used to stain the samples. For ABC reactions, the sections were fixed with 4% formaldehyde in phosphate-buffered saline (PBS) for 5 min at room temperature and washed in PBS. Sections were pre-incubated for 30 min in normal goat serum (1 : 10) and incubated for 36 h at 4 °C in the primary antibody and for 1 h in biotinylated anti-rabbit IgG diluted 1 : 200. The sections were then incubated for 1 h in ABC complex and visualized in 0.03% diaminobenzidine (DAB) (Dojin, Kumamoto, Japan) containing 0.005% peroxide. The specificity of the immunoreactivity was verified by omitting the primary antibody, replacing the polyclonal antibody with

**Table 1.** Clinical summary of the patients

| Patient | Diagnosis | Sex | Age(y) of onset | Age(y) at biopsy | Clinical symptoms at biospy | Serum CK |
|---|---|---|---|---|---|---|
| 1 | DMD | M | 0.8 | 1.2 | Difficulty in standing up | 22000 |
| 2 | DMD | M | 2 | 2.8 | Frequent falling down | 14250 |
| 3 | DMD | M | 1.5 | 3.5 | Frequent falling down | 16130 |
| 4 | DMD | M | 2 | 4 | Abnormal gait | 21000 |
| 5 | DMD | M | 3 | 4.4 | Unsteady gait | 14690 |
| 6 | DMD | M | 4 | 5 | Frequent falling down | 14550 |
| 7 | DMD | M | 3 | 8 | Abnormal gait | 13600 |
| 8 | DMD | M | 3 | 15 | Frequent falling down | 2428 |
| 9 | FCMD | F | 0.1 | 0.7 | Hypotonia | 3600 |
| 10 | FCMD | M | 0.1 | 0.7 | Floppy infant | 2726 |
| 11 | FCMD | M | 0.3 | 1 | Motor delay | 11850 |
| 12 | FCMD | M | 0.5 | 2.7 | Motor delay | 6009 |
| 13 | FCMD | M | 0.1 | 7 | Severe developmental delay | 3930 |
| 14 | FCMD | F | 0.5 | 18 | Motor delay | 300 |
| 15 | CMD | M | 0.1 | 0.7 | Floppy infant | 2463 |
| 16 | CMD | M | 0.3 | 0.7 | Delayed head control | 6092 |
| 17 | CMD | F | 1.5 | 2.2 | Gait disturbance | 965 |
| 18 | BMD | M | no symptom | 5 | Hypercknemia | 1847 |
| 19 | BMD | M | 5 | 7 | Muscle pain | 3844 |
| 20 | BMD | M | 5 | 11 | Slow runner | 5159 |
| 21 | BMD | M | 6 | 11 | Leg pain | 5159 |
| 22 | BMD | M | no symptom | 13 | Hypercknemia | 5000 |

DMD: Duchenne muscular dystrophy, FCMD: Fukuyama type congenital muscular dystrophy, CMD: merosin-positive congenital muscular dystrophy, BMD: Becker muscular dystrophy.

non-immune rabbit IgG (Zymed, San Francisco, CA, USA) at the same concentration, and absorbing the primary polyclonal anti-PDGFR alpha or beta antibody with recombinant PDGFR alpha or beta peptides (sc-338p and sc-339p; Santa Cruz Biotechnology, Santa Cruz, CA, USA). Omission of the primary antibody and replacement of polyclonal antibodies with non-immune IgG abolished reactivity. Absorption of anti-PDGFR alpha or beta antibody (0.5 μg/ml) with PDGFR alpha or beta peptide (final concentration 100 μg/ml) overnight at 4 °C resulted in complete blocking of the reaction products.

For immunohistochemical analysis of PDGFR alpha and beta in dystrophic mouse models, we used hamstring muscles from B-10 mice as a control, *dy* mice as a progressive and fibrotic model, and *mdx* mice as a non-fibrotic model at 16 weeks old. The *dy* mice are known to be a merosin-deficient CMD model and *mdx* mice are known to be a DMD model [18]. Muscles were obtained after neck dislocation and were immediately frozen in isopentane and stored at −80 °C until used. Immunohistochemical studies were performed with the same antibodies that were used for human muscle biopsies using the ABC reaction. The protocol for the use of mouse tissue was approved by the Animal Experimentation Committee of the School of Medicine, Tohoku University.

Double or triple fluorescence labelling was used to co-localize PDGF-A, PDGF-B, PDGFR alpha or PDGFR beta with desmin, α-bungarotoxin (α-BT), CD31, CD68, prolyl 4-hydroxylase (P-4-H) or Hoechst 33342. For double fluorescence staining, sections were fixed with 4% formaldehyde in PBS for 5 min at room temperature, washed in PBS, and pre-incubated for 30 min in normal donkey serum diluted 1 : 10. Sections were incubated for 36 h at 4 °C in the appropriately diluted mixture of primary antibodies and then incubated for 1 h in a mixture of secondary antiserum containing Texas Red-labelled donkey anti-rabbit IgG and Cy2-labelled donkey anti-mouse IgG (Jackson Immuno Res, West Grove, PA, USA) diluted at 1 : 200. To visualize intramuscular nuclei, some sections were triple labelled by incubation in 10 μg/ml Hoechst 33342 (Molecular Probes, Eugene, OR, USA) for 5 min. Monoclonal antibodies against desmin (1 : 100) (Zymed, San Francisco, CA, USA), CD31 (1 : 100) (Santa Cruz Biotechnology, Santa Cruz, CA, USA), CD68 (1 : 100), and P-4-H (1 : 100) (Dako, Glostrup, Denmark) were used to identify regenerating fibres, vessels, macrophages, and fibroblasts actively producing collagen [19], respectively. Neuromuscular junctions (NMJs) were identified with tetramethylrhodamine-labelled α-BT (Molecular Probes, Eugene, OR, USA) diluted at 1 : 1000. Immunofluorescence images were observed with a fluorescence microscope and were captured separately from the same area with a CCD camera connected to a personal computer. The images were combined using a Q550CW fluorescence imaging system (Leica, Cambridge, UK). The staining intensity of muscle fibres and extracellular matrix (ECM) was scored separately by reviewing the entire tissue section with a semi-quantitative scale: 0, no staining; 0.5, trace staining; 1, light staining; 2, moderate staining; and 3, intense staining.

To evaluate endomysial fibrosis, serial sections were stained for cytochrome c oxidase and three images that included only the endomysial area (0.403 $mm^2$ in total) were captured at ×200 magnification with a CCD camera connected to a personal computer. The endomysial interstitial area of each image (ie the cytochrome c oxidase-negative area) was measured using a colour image computer analyser (MacSCOPE, version 2.5, Mitani Corp, Hukui, Japan) and the mean value of three images was determined as the endomysial interstitial area for each sample, which is expressed as a percentage in Table 2.

For immunoblot analysis, ten 10-μm-thick cryosections of three FCMD muscles biopsied in early infancy (two) and at an advanced stage (one) and one control muscle biopsy were collected on ice; homogenized in 10 mM Tris–HCl (pH 7.4) containing 150 mM KF, 15 mM EDTA, 1 mM phenylmethylsulphonyl fluoride, 10 mg/ml leupeptin, 1 mM benzamidine, and 1 μm/ml 2-mercaptoethanol; and centrifuged at 10 000 *g* for 15 min at 4 °C. For SDS-PAGE, equal amounts of muscle protein [10 μg diluted in SDS incubation medium: 62.5 mM Tris–HCl (pH 6.8), 2% SDS, 10% glycerol, 5% 2-mercaptoethanol, and 0.02% bromophenol blue] were loaded on the gel (12.5% acrylamide) according to the method of Laemmli [20]. The upper and lower running buffers contained 25 mM Tris (base), 192 mM glycine, and 0.1% SDS, and the gel was run at 200 V for 30 min. The proteins were then transferred onto nitrocellulose sheets for 1 h at 4 °C at 100 V using a transfer buffer containing 182 mM glycine, 6 mM Tris, and 20% methanol at pH 8.2. After blocking the blots in 5% non-fat dry milk in PBST (PBS, pH 7.4, containing 0.1% Tween-20) for 2 h, they were incubated with the primary antibody (anti-PDGFR beta; 1 : 100) overnight and then incubated with horseradish peroxidase-conjugated donkey anti-rabbit IgG (1 : 1500; Chemicon, Temecula, CA, USA) for 1 h. Immunoreactive proteins were visualized using a DAB kit (Vector, Burlingame, CA, USA) or with enhanced chemiluminescence (Bio-Rad, Hercules, CA, USA).

## Results

### Human muscular dystrophy (Figures 1–4 and Table 2)

#### PDGF-A immunolocalization (Figures 1 and 2)

In normal muscle biopsies, trace PDGF-A immunoreactivity was observed in vascular smooth muscle (Figure 1A). The neuromuscular junctions in all muscles were stained positively, as described in our

**Table 2.** Results of immunolocalization of PDGF-A, PDGF-B, PDGFR alpha, and PDGFR beta

| Patient | Age (y) at biopsy | Diagnosis | PDGF-A | | PDGF-B | | PDGFR alpha | | PDGFR beta | | Interstitial Area (%) |
|---|---|---|---|---|---|---|---|---|---|---|---|
| | | | MF[1] | ECM | MF[1] | ECM | MF[1&2] | ECM | MF[1] | ECM | |
| 1 | 1.2 | DMD | 0.5 | 0.5 | 2 | 1 | 2 | 0.5 | 0 | 2 | 14.9 |
| 2 | 2.8 | DMD | 0.5 | 1 | 1 | 2 | 2 | 0.5 | 0 | 3 | 20.5 |
| 3 | 3.5 | DMD | 1 | 1 | 1 | 1 | 2 | 1 | 0 | 2 | 16.6 |
| 4 | 4 | DMD | 0.5 | 1 | 0.5 | 1 | 1 | 0.5 | 0 | 2 | 16.7 |
| 5 | 4.4 | DMD | 1 | 0.5 | 1 | 1 | 2 | 1 | 0 | 2 | 20.7 |
| 6 | 5 | DMD | 0.5 | 0.5 | 1 | 1 | 0.5 | 0.5 | 0 | 3 | 15.8 |
| 7 | 8 | DMD | 1 | 0.5 | 1 | 1 | 1 | 1 | 0 | 2 | 16.3 |
| 8 | 15 | DMD | 0.5 | 0.5 | 0 | 0.5 | 0 | 0 | 0 | 1 | 37.3 |
| 9 | 0.7 | FCMD | 1 | 0.5 | 2 | 2 | 2 | 2 | 0 | 3 | 29.6 |
| 10 | 0.7 | FCMD | 1 | 0.5 | 2 | 2 | 2 | 1 | 0 | 3 | 40.9 |
| 11 | 1 | FCMD | 0.5 | 0.5 | 1 | 0.5 | 0.5 | 2 | 0 | 3 | 40.7 |
| 12 | 2.7 | FCMD | 0.5 | 0.5 | 0.5 | 0.5 | 0.5 | 0.5 | 0 | 1 | 67.8 |
| 13 | 7 | FCMD | 0 | 0.5 | 0 | 0.5 | 0 | 0 | 0 | 0 | 52.6 |
| 14 | 18 | FCMD | 0 | 0 | 0 | 0 | 0 | 0 | 0 | 0 | 92 |
| 15 | 0.7 | CMD | 1 | 0.5 | 2 | 1 | 2 | 0.5 | 0 | 2 | 49.8 |
| 16 | 0.7 | CMD | 1 | 0.5 | 2 | 1 | 2 | 1 | 0 | 3 | 43.3 |
| 17 | 2.2 | CMD | 1 | 0.5 | 2 | 1 | 2 | 1 | 0 | 2 | 49.8 |
| 18 | 5 | BMD | 0 | 0 | 0 | 0.5 | 0.5 | 0 | 0 | 0 | 11.1 |
| 19 | 7 | BMD | 0 | 0 | 0 | 0 | 0.5 | 0 | 0 | 0 | 6.4 |
| 20 | 11 | BMD | 0 | 0 | 0 | 0 | 0.5 | 0 | 0 | 0 | 7.5 |
| 21 | 11 | BMD | 0.5 | 0 | 0.5 | 0.5 | 0.5 | 0 | 0 | 0 | 6.2 |
| 22 | 13 | BMD | 0.5 | 0 | 0.5 | 0.5 | 0.5 | 0 | 0 | 0 | 8.8 |
| 23 | 1.5 | normal | 0 | 0 | 0 | 0 | 0 | 0 | 0 | 0 | 8.8 |
| 24 | 2.2 | normal | 0 | 0 | 0 | 0 | 0 | 0 | 0 | 0 | 6.5 |
| 25 | 2.3 | normal | 0 | 0 | 0 | 0 | 0 | 0 | 0 | 0 | 7.5 |
| 26 | 3 | normal | 0 | 0 | 0 | 0 | 0 | 0 | 0 | 0 | 5.2 |
| 27 | 3.5 | normal | 0 | 0 | 0 | 0 | 0 | 0 | 0 | 0 | 6.3 |
| 28 | 5 | normal | 0.5 | 0 | 0 | 0 | 0 | 0 | 0 | 0 | 4.5 |
| 29 | 6.5 | normal | 0.5 | 0 | 0 | 0 | 0 | 0 | 0 | 0 | 8.8 |
| 30 | 8 | normal | 0 | 0 | 0 | 0 | 0 | 0 | 0 | 0 | 5.6 |
| 31 | 12 | normal | 0 | 0 | 0 | 0 | 0 | 0 | 0 | 0 | 7.8 |
| 32 | 13 | normal | 0 | 0 | 0 | 0 | 0 | 0 | 0 | 0 | 8.6 |

MF: muscle fibers.
ECM: extracellular matrix.
MF[1]: immunolocalization except for regenerating fibers.
MF[2]: sarcolemmal immunolocalization.
PDGF: platelet-derived growth factor.
PDGFR: platelet-derived growth factor receptor.
Intensity of immunostaining: 0; no staining, 0.5; trace staining, 1; light staining, 2; moderate staining, 3; intense staining.

previous report [21]. Necrotic fibres with mononuclear cell infiltration showed positive immunoreactivity (Figure 1B) in all dystrophic muscles examined. The cytoplasm and nuclei of regenerating muscle fibres were strongly positive in all dystrophic muscles (Figure 1C); this was confirmed by double labelling with PDGF-A and desmin (Figures 2A and 2B). Triple labelling with PDGF-A, CD68, and Hoechst 33342 (Figures 2C and 2D) demonstrated co-localization of PDGF-A immunoreactivity on the regenerating fibre nuclei and macrophages infiltrating the endomysium. However, elderly CMD and DMD cases with advanced fibrosis showed trace or no PDGF-A reactivity (Table 2).

### PDGF-B immunolocalization (Figures 1 and 2)

In normal muscle biopsies, trace PDGF-B immunoreactivity was observed in muscle fibre nuclei and vascular smooth muscle (Figure 1E). Double immunolabelling with PDGF-B and $\alpha$-BT showed that neuromuscular junctions in all muscles were positively stained (Figures 2H and 2I). Mononuclear cells that infiltrated in and around necrotic fibres showed intense positivity for PDGF-B in DMD, CMD, and BMD (Figures 1F–1H). Double labelling with antibodies against PDGF-B and CD68 showed exclusive PDGF-B co-localization (Figures 2E–2G) on almost all macrophages in the endomysium. The vascular walls and muscle fibre nuclei of non-regenerating fibres in dystrophic muscles were lightly to moderately immunostained (Figures 1F–1H and 2E). The cytoplasm and nuclei of regenerating muscle fibres, which were characterized by strong desmin immunoreactivity (data not shown), showed intense staining in all dystrophic muscles. However, elderly CMD and DMD cases with advanced fibrosis showed trace or no PDGF-B reactivity (Table 2).

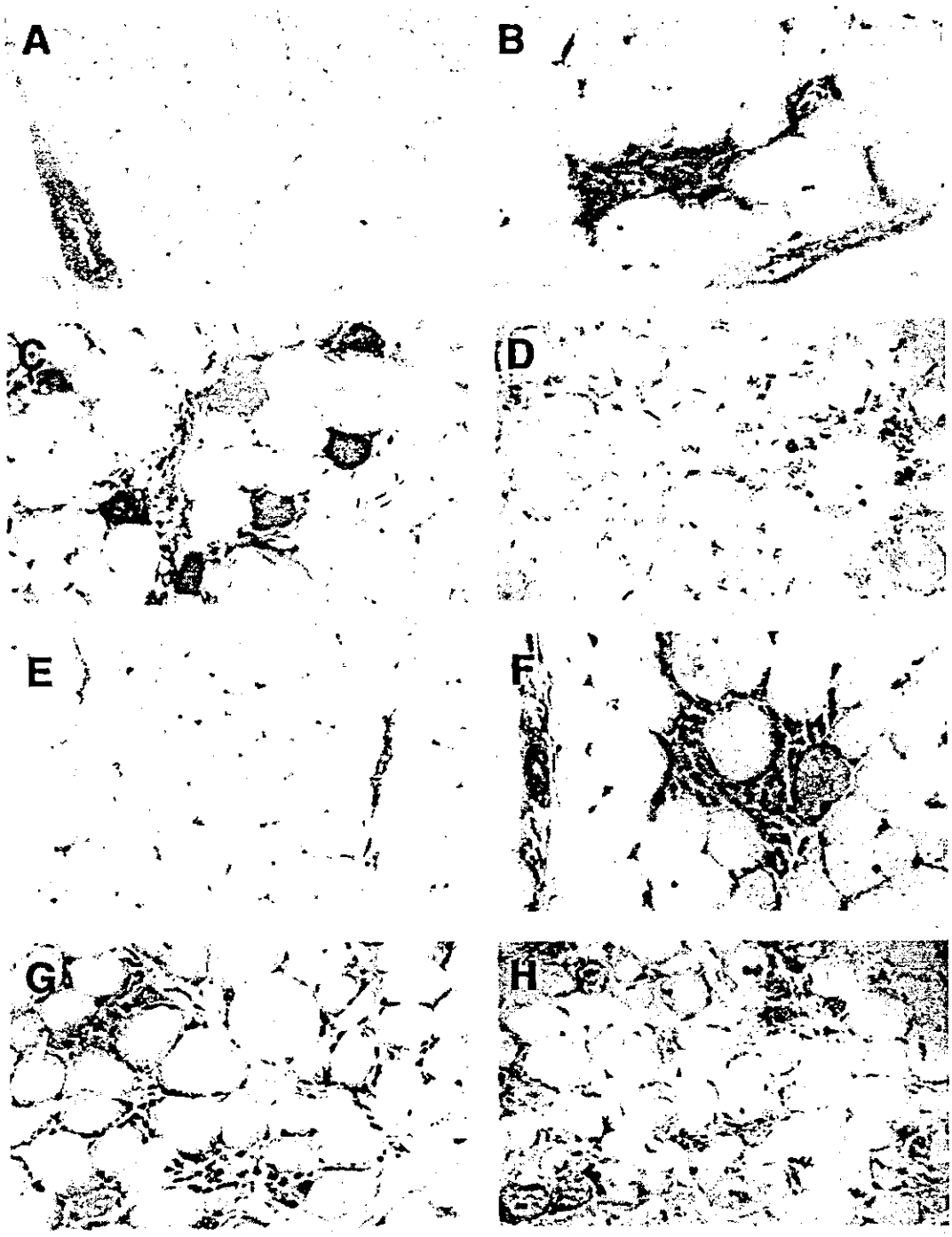


**Figure 1.** Immunolocalization of PDGF-A (A–D) and PDGF-B (E–H) in biopsied muscles from control (A, E), BMD (B, F), DMD (C, G), and FCMD (D, H). PDGF-A and PDGF-B immunoreactivity was prominent in infiltrating cells, regenerating muscle fibres, and muscle fibre nuclei in dystrophic muscles

#### PDGFR alpha immunolocalization (Figures 3 and 4)

In control muscle biopsies, moderate PDGFR alpha immunoreactivity was observed in neuromuscular junctions [20] and trace immunoreactivity was observed around muscle fibre nuclei (Figure 3A). Some sections showed moderate staining of the perimysial connective tissue. In the DMD and CMD muscle fibres examined, muscle fibre sarcolemma was lightly immunostained in 20–40% of muscle fibres (Figures 3B and 3D), whereas in BMD muscle fibres, 1–3% of muscle fibre sarcolemma was faintly immunostained. The cytoplasm of necrotic and regenerating muscle fibres was moderately to intensely stained in dystrophic muscles (Figures 4A and 4B) and nuclei of non-regenerating muscle fibres were also lightly to moderately stained. The endomysium of CMD cases biopsied at an early stage showed moderate staining of the endomysium (Figure 3D).

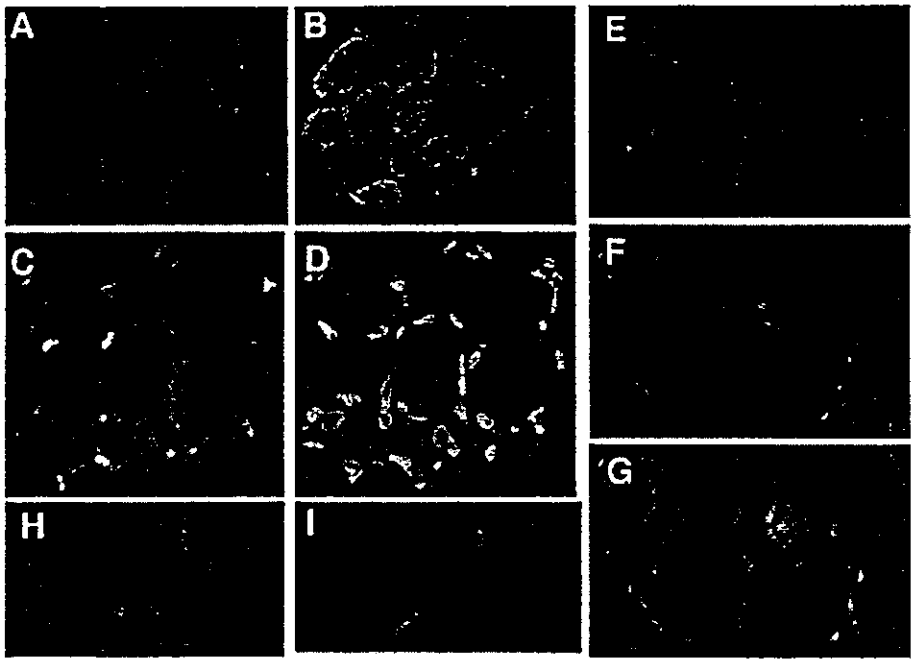


**Figure 2.** Immunolabelling of DMD muscles. (A, B) PDGF-A was immunolocalized in regenerating muscle fibres that showed strong desmin immunoreactivity and in their nuclei [double labelling; A: PDGF-A (red); B: desmin (green)]. (C, D) Infiltrating macrophages were positive for PDGF-A (yellow). Nuclei of regenerating fibres were intensely positive for PDGF-A and nuclei of non-regenerating fibres were also lightly positive [triple labelling; C: merged PDGF-A (red)/CD68 (green); D: merged PDGF-A (red)/Hoechst 33342 (blue)]. (E–G) PDGF-B was strongly expressed in the intramuscular vessels and phagocytic macrophages (yellow) infiltrating into the necrotic fibre [double labelling; E: PDGF-B (red); F: CD68 (green); G: merged PDGF-B/CD68]. (H–I) PDGF-B co-localized with α-BT at the neuromuscular junctions [double labelling; H: PDGF-B (green); I: α-BT (red)]

However, relatively elderly CMD and DMD cases with advanced fibrosis showed very poor PDGFR alpha reactivity (Table 2). Double labelling with antibodies against PDGFR alpha and CD68 demonstrated that PDGFR alpha was intensely expressed in macrophages infiltrating in and around necrotic fibres (Figure 4C). Double immunolabelling with antibodies against PDGFR alpha and P-4-H demonstrated that P-4-H-positive activated fibroblasts were clearly positive for PDGFR alpha in DMD and CMD muscle (Figure 4D).

#### PDGFR beta immunolocalization (Figures 3 and 4)

In control muscle biopsies, light PDGFR beta immunoreactivity was observed in neuromuscular junctions (data not shown), capillaries, and vascular smooth muscle (Figures 3E, 4E, and 4F). The cytoplasm of strongly desmin-positive regenerating muscle fibres showed light staining in dystrophic muscles (Figures 4G and 4H). Triple labelling with PDGFR beta, CD68, and Hoechst 33342 demonstrated that PDGFR beta was expressed partly by CD68-positive macrophages infiltrating the endomysium and by other mononuclear cells in the interstitium (Figures 4I and 4J). The most remarkable finding was the intense immunoreactivity of the endomysium in DMD and CMD muscles (Figures 3F, 3H, and 3I). However, there was no endomysial PDGFR beta expression in BMD muscles (data not shown). Compared with DMD muscle, PDGFR beta expression was clearly predominant in CMD muscles biopsied in early infancy (Figures 3H and 3I). Double immunolabelling with antibodies against PDGFR beta and P-4-H demonstrated that P-4-H-positive activated fibroblasts were exclusively PDGFR beta-positive in DMD and CMD muscle (Figures 4K–4M). In contrast to CMD and DMD muscles biopsied in early infancy, CMD and DMD muscles with advanced fibrosis showed no or faint reactivity against PDGFR beta (Figure 3J).

#### Immunoblots for PDGFR beta (Figure 5)

Immunoblots of muscle extracts from FCMD patients biopsied in early infancy revealed a clear immunoreactive band with an apparent molecular mass of 180 kD corresponding to the 180 kD PDGFR beta, while muscle extracts from a FCMD patient biopsied at an advanced stage and the control patient lacked this 180 kD immunoreactive band. These findings are consistent with the results of the immunohistochemical analysis. Owing to the small size of the diagnostic muscle biopsies, we did not have sufficient material to perform immunoblotting with anti-PDGFR alpha, PDGF-A, or PDGF-B antibodies.

### Mouse muscular dystrophy (Figure 6)

In B-10 mouse muscle, PDGFR alpha was faintly immunolocalized on muscle sarcolemma and intensely localized at neuromuscular junctions (Figure 6A). In *mdx* mouse muscle, PDGFR alpha was immunolocalized lightly to moderately on the sarcolemma of

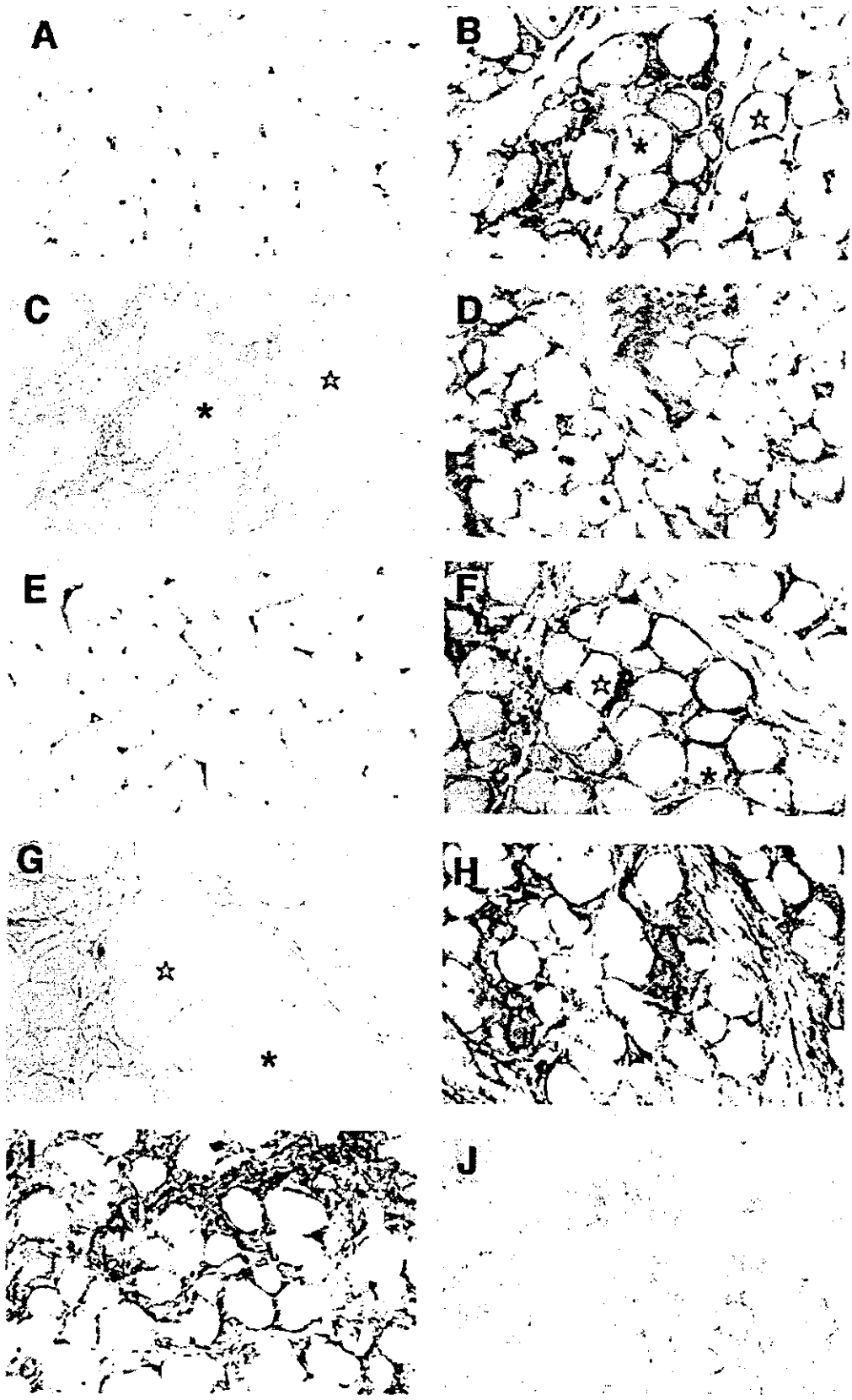


**Figure 3.** Immunolocalization of PDGFR alpha (A–D) and PDGFR beta (E–J) in biopsied muscles from control (A, E), DMD (B, C, F, G), FCMD (D, H, J), and merosin-positive CMD (I). Immunoreactivity against PDGFR alpha (B) and beta (F) was completely abolished after absorption with antigen peptides (C, G). Immunoreactivity against both PDGFRs in CMD muscle biopsied in early infancy was marked in the endomysium (D, H, I), while FCMD muscles biopsied from elderly cases with advanced fibrosis showed a lack of immunoreactivity (J)

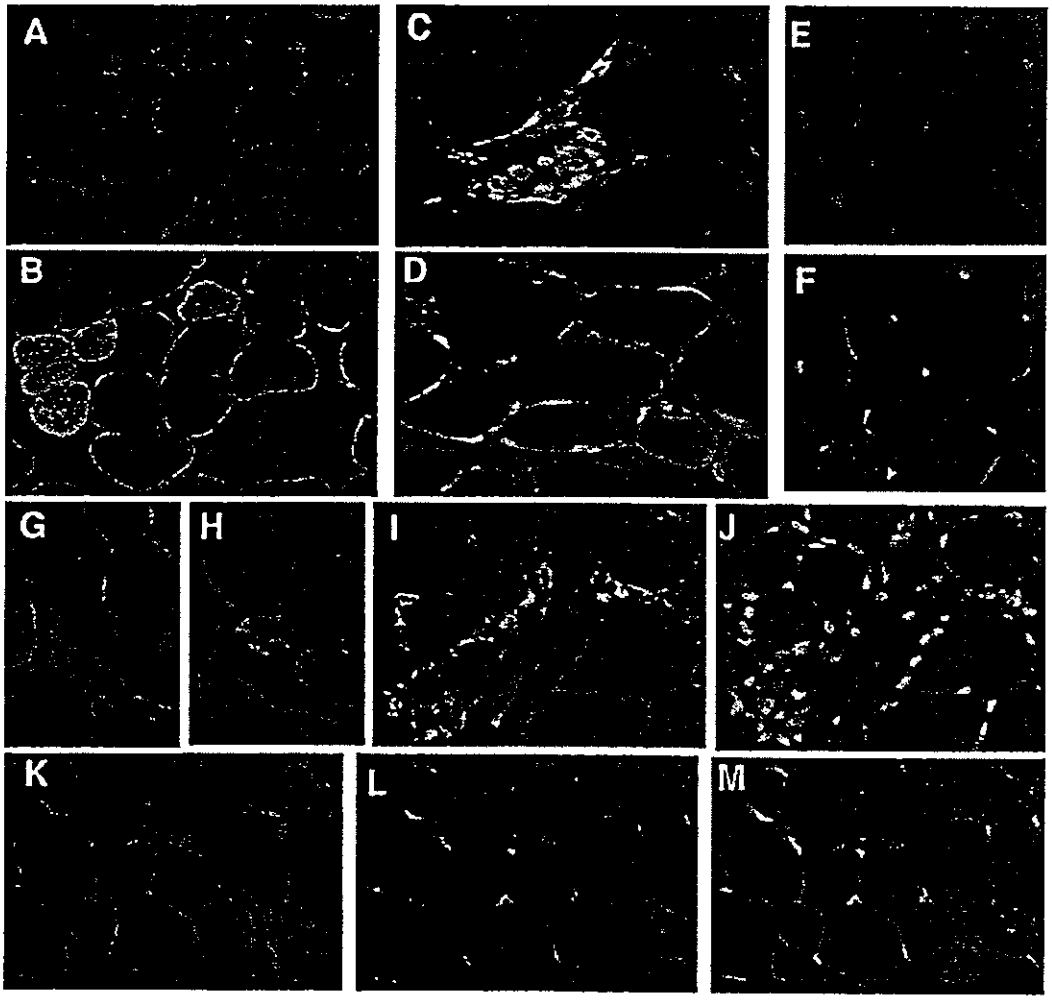


**Figure 4.** Double and triple labelling of PDGFR alpha and beta in DMD muscles (A–D, G–M) and control (E, F). (A, B) PDGFR alpha was expressed in regenerating fibres with remarkable desmin positivity and necrotic fibres without desmin immunoreactivity [double labelling; A: PDGFR alpha (red); B: desmin (green)]. (C) PDGFR alpha was co-localized with CD68 in the macrophages infiltrating into and around necrotic fibres (yellow) [merged PDGFR alpha (red)/CD68 (green)]. (D) PDGFR alpha was co-localized with a marker of activated fibroblasts, P-4-H (yellow) [double labelling; merged PDGFR alpha (red)/P-4-H (green)]. (E, F) PDGFR beta was co-localized with CD31 at the intramuscular capillaries [double labelling; E: PDGFR beta (red); F: CD31 (green)]. (G, H) PDGFR beta was lightly expressed in regenerating fibres with remarkable desmin positivity, while vessels and interstitium showed intense staining [double labelling; G: PDGFR beta (red); H: desmin (green)]. (I, J) PDGFR beta was co-localized with CD68 in some macrophages (yellow) in the interstitium. Other mononuclear interstitial cells were also positively stained [triple labelling; I: merged PDGFR beta (red)/CD68 (green); J: merged PDGFR beta (red)/Hoechst 33342 (blue)]. (K-M) PDGFR beta was exclusively co-localized with activated fibroblasts in the endomysium (yellow) [double labelling; K: PDGFR beta (red); L: P-4-H (green); M: merged PDGFR beta/P-4-H]

regenerating muscle fibres (Figure 6B). The cytoplasm and internal nuclei of regenerating muscle fibres were also lightly stained. In *dy* mouse muscle, PDGFR alpha was moderately to intensely immunolocalized in the endomysium and muscle fibre sarcolemma also showed light to moderate staining. Cells distributed in the endomysium and nuclei of regenerating fibres were intensely immunostained (Figure 6C).

PDGFR beta immunostaining showed light positivity in the vessels and interstitium in B-10 mice (Figure 6D), while in *mdx* mice, the cytoplasm of regenerating muscle fibres and endomysium were lightly stained (Figure 6E). In *dy* mice, the interstitium and cells distributed in the endomysium were intensely stained with PDGFR beta, as seen in human DMD and CMD muscles (Figure 6F). Regenerating fibre cytoplasm was also lightly immunostained.

## Discussion

Previous studies have shown that TGF$\beta$1 and bFGF are involved in the pathophysiology of human muscular dystrophy, particularly in muscle fibrosis [6–8,22]. However, their distinct localization in dystrophic muscles had not been studied in detail with double immunolocalization. Moreover, receptors for these growth factors had not been studied, except for FGF receptor 4, which was expressed in one patient with FSHD [22]. Our study has shown that PDGF

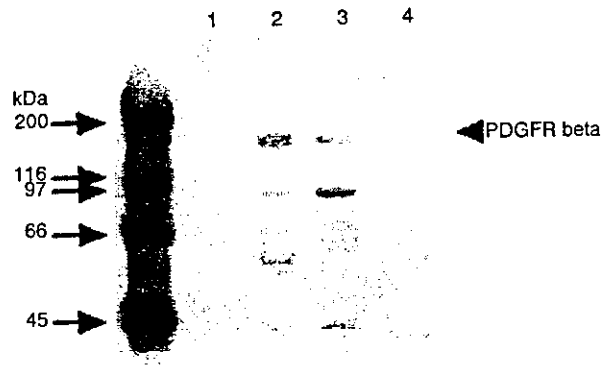


**Figure 5.** Immunoblot analysis of PDGFR beta in extracts from muscles from the normal control (lane 1), FCMD biopsied in early infancy (lanes 2 and 3), and FCMD biopsied in an elderly patient (lane 4). A 180 kD band corresponding to PDGFR beta protein is clearly present in the muscles of cases with early FCMD, while the muscles of normal controls and cases with advanced FCMD lacked a recognizable band for PDGFR beta

and its receptors are involved in the pathophysiology of dystrophic muscles. Using double immunohistochemistry, we have shown that in dystrophic muscles, PDGF is immunolocalized in infiltrating macrophages, regenerating muscle fibres, and myofibre nuclei, and that PDGFR is immunolocalized in infiltrating macrophages, regenerating and necrotic muscle fibres, interstitial fibroblasts, and muscle fibre sarcolemma.

It is well known that fibrotic changes occur in the muscle tissue of *dy* mice in the early stage of development, while *mdx* mice show minimal fibrotic changes throughout their life, despite their lack of dystrophin [18]. There has been no reasonable explanation so far why *mdx* mice have a very slight clinical alteration, unlike DMD muscle. In the present study, PDGFR alpha and beta were immunolocalized markedly in the endomysium of *dy* mice, compared with *mdx* mice. These results were comparable to the results for human dystrophic muscles. The relative abundance of interstitial PDGFR expression might contribute to the tissue fibrosis seen in *dy* mice.

The present study is the first report of significant PDGFR beta and alpha overexpression in the endomysium in human and mouse dystrophic muscles, particularly in *dy* mouse muscle. The present study is also the first to demonstrate that P-4-H-positive activated fibroblasts in the endomysium clearly express PDGFR alpha and beta. These findings demonstrate that fibroblasts in the endomysium of dystrophic muscles remain activated partly through paracrine regulation by PDGF. Interestingly, PDGF and its receptors are remarkably expressed in DMD and CMD muscles biopsied at an early stage of disease progression. However, immunoreactivity was almost abolished in DMD and CMD muscles biopsied from elderly patients with advanced fibrosis. This was clearly confirmed by immunoblot analysis, as shown in Figure 5. These findings suggest that PDGF and its receptors are significantly involved in the active stage of tissue destruction and are associated with the initiation or promotion of muscle fibrosis. These processes might occur in concert with other cytokines and growth factors, since *in vitro* studies have shown that (1) TGF$\beta$ increases PDGF-B mRNA transcription in microvascular endothelial cells [23] and also increases PDGFR beta transcription in human liver fat-storing cells [24]; (2) TGF$\beta$ up-regulates PDGFR alpha expression in human scar fibroblasts and fibroblasts from scleroderma patients [25]; (3) bFGF up-regulates PDGFR alpha expression in smooth muscle cells [26]; (4) PDGF-BB up-regulates PDGFR alpha and beta expression in human foreskin fibroblasts [27]; and (5) tissue fibroblasts are activated and transformed

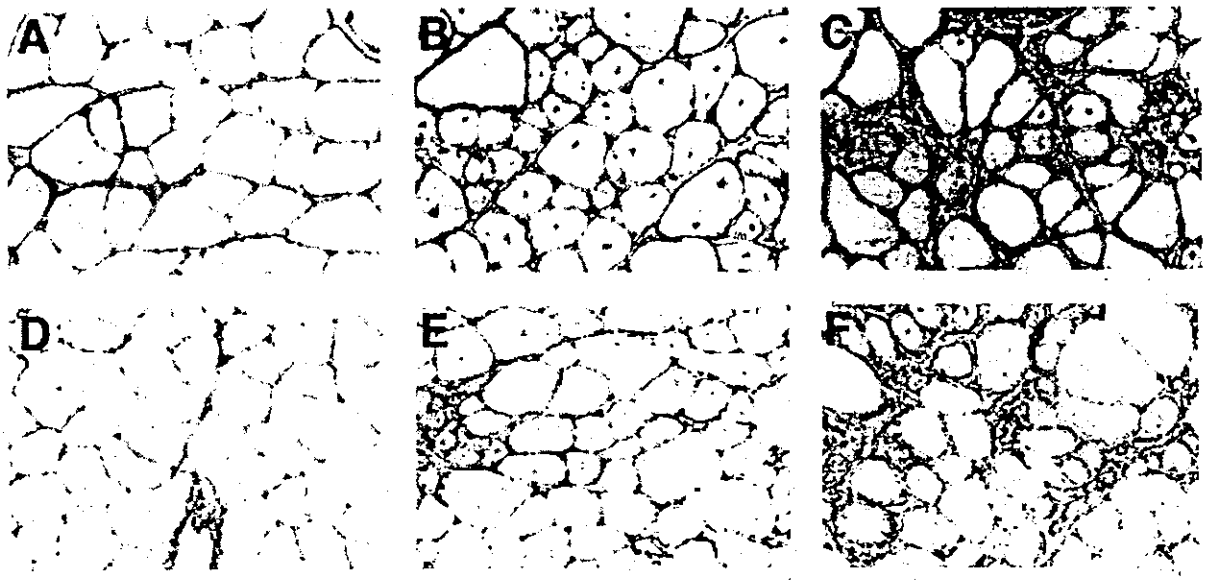


**Figure 6.** Immunolocalization of PDGFR alpha (A–C) and beta (D–F) in muscles of B-10 (A, D), *mdx* (B, E), and *dy* (C, F) mice. Immunoreactivities of the endomysium for both PDGFRs were prominent in *dy* mice compared with those of *mdx* mice

to myofibroblasts by TGF$\beta$ and PDGF [28]. In fibrosis, PDGF-BB and PDGFR alpha or beta contribute to scleroderma formation and liver fibrosis, while PDGF-AA and PDGFR alpha contribute to pulmonary fibrosis [29]. In dystrophic muscles, our study clearly shows that fibrosis is controlled by both PDGFR alpha and beta signalling.

Previous studies have shown that necrotic muscle fibres release chemotactic factors to attract polymorphonuclear leukocytes and macrophages, while macrophages release factors that induce a chemotactic response in satellite cells [30–32]. Satellite cells migrate to the necrotic area and begin to proliferate, and muscle fibre regeneration is accomplished after the fusion of those cells [30]. In all the dystrophic muscles examined in this study, PDGF-A and PDGF-B were strongly immunolocalized in the cytoplasm and nuclei of regenerating muscle fibres and in macrophages infiltrating into necrotic fibres. PDGFR alpha and beta were also immunolocalized in regenerating muscle fibre cytoplasm and macrophages. Previous *in vitro* studies using mouse and porcine cultured myoblasts demonstrated that the PDGF-BB/PDGFR beta signalling pathway is mainly involved in myoblast proliferation [13,33]. However, our study shows that PDGF-A and PDGF-B peptides and their beta and alpha receptors are expressed equally in regenerating fibres. This suggests that both chains have autocrine and paracrine roles in muscle fibre regeneration or satellite cell chemotaxis in dystrophic skeletal muscles.

PDGFR alpha was overexpressed in the non-regenerating muscle fibre sarcolemma in DMD and CMD, but faintly expressed in BMD. However, it remains to be clarified whether PDGFR alpha has any physiological function in non-regenerating dystrophic muscle fibres. Utrophin, an autosomal homologue to dystrophin, preferentially accumulates at the postsynaptic membrane in normal muscle fibres [34], but is overexpressed at the sarcolemma of DMD muscle fibres [35]. Recent research revealed that the up-regulation of utrophin functionally compensates for the lack of dystrophin in *mdx* mice [36]. Since PDGFR alpha also accumulates at the neuromuscular junction in normal muscle, it will be interesting to study the functional relationship between PDGFR alpha and dystrophin-related proteins.

The present study demonstrates that PDGF-A, PDGF-B, PDGFR alpha, and PDGFR beta are all immunolocalized at the neuromuscular junction, suggesting that they have physiological roles in the interaction between the presynaptic and postsynaptic components [21]. Similar roles have been reported for other growth factors expressed at the neuromuscular junction, such as bFGF, TGF$\beta$1 and TGF$\beta$2 [37–39].

We have demonstrated that PDGF and its receptors are related to muscle fibre regeneration and fibrosis, and that they may be important for the progression of muscular dystrophy. Recently, the *in vivo* transfer of the PDGFR beta extracellular domain effectively ameliorated bleomycin-induced pulmonary fibrosis [40]. Other PDGF antagonists have also been used to reduce pathological changes induced by PDGF [41,42]. These methods should also be tested in models of muscular dystrophy.

## Acknowledgement

This work was supported partly by funding from The Morinaga Hoshi-kai, Japan.

## References

1. Mastaglia FL, Kakulas BA. Regeneration in Duchenne muscular dystrophy: a histological and histochemical study. *Brain* 1969; **92**: 809–818.
2. Cuzzato G. Consideration about a possible role played by connective tissue proliferation and vascular disturbances in the pathogenesis of progressive muscular dystrophy. *Eur Neurol* 1968; **1**: 158–179.
3. Ionasescu V, Lora-Braud C, Zellweger H, *et al.* Fibroblast cultures in Duchenne muscular dystrophy. Alterations in synthesis and secretion of collagen and noncollagen proteins. *Acta Neurol Scand* 1977; **55**: 407–417.
4. Melone MAB, Peluso G, Petillo O, *et al.* Defective growth *in vitro* of Duchenne muscular dystrophy myoblasts: the molecular and biochemical basis. *J Cell Biochem* 1999; **76**: 118–132.
5. Melone MAB, Peluso G, Galderisi U, *et al.* Increased transcription of IGF binding protein-5 (IGFBP-5) mRNAs in Duchenne muscular dystrophy (DMD) fibroblasts correlates with the fibroblast induced down regulation of DMD myoblast proliferation: an *in vitro* analysis. *Neurology* 2000; **54**(Suppl 3): A438–A439.
6. Bernasconi P, Torchiana E, Confalonieri P, *et al.* Expression of transforming growth factor-beta1 in dystrophic patient muscles correlates with fibrosis. *J Clin Invest* 1995; **96**: 1137–1144.
7. Bernasconi P, Di Blasi C, Mora M, *et al.* Transforming growth factor-beta 1 and fibrosis in congenital muscular dystrophies. *Neuromuscular Disord* 1999; **9**: 28–33.
8. Yamazaki M, Minota S, Sakurai H, *et al.* Expression of transforming growth factor-beta1 and its relation to endomysial fibrosis in progressive muscular dystrophy. *Am J Pathol* 1994; **144**: 221–226.
9. D'Amore PA, Brown JRH, Ku P-T, *et al.* Elevated basic fibroblast growth factor in the serum of patients with Duchenne muscular dystrophy. *Ann Neurol* 1994; **35**: 362–365.
10. Ishitobi M, Haginoya K, Zhao Y, *et al.* Elevated plasma levels of transforming growth factor beta1 in patients with muscular dystrophy. *NeuroReport* 2000; **11**: 4033–4035.
11. Heldin C-H, Westermark B. Platelet-derived growth factor: mechanism of action and possible *in vivo* function. *Cell Regul* 1990; **1**: 555–566.
12. Ross R, Raines EW, Bowen-Pope DF. The biology of platelet-derived growth factor. *Cell* 1986; **46**: 155–169.
13. Seifert RA, Hart CE, Phillips PE, *et al.* Two different subunits associate to create isoform-specific platelet-derived growth factor receptors. *J Biol Chem* 1989; **264**: 8771–8778.
14. Jin P, Rahm M, Claesson-Welsh L, *et al.* Expression of PDGF A-chain and B-receptor genes during rat myoblast differentiation. *J Cell Biol* 1990; **110**: 1665–1672.
15. Sejersen T, Betsholtz C, Sjolund M, *et al.* Rat skeletal myoblasts and arterial smooth muscle cells express the gene for the A chain but not the gene for the B chain (c-sis) of platelet-derived growth factor (PDGF) and produce a PDGF-like protein. *Proc Natl Acad Sci U S A* 1986; **83**: 6844–6848.
16. Tidball JG, Spencer MJ, Pierre BA. PDGF-receptor concentration is elevated in regenerative muscle fibers in dystrophin-deficient muscle. *Exp Cell Res* 1992; **203**: 141–149.
17. Jin P, Sejersen T, Ringertz NR. Recombinant platelet-derived growth factor-BB stimulates growth and inhibits differentiation of rat L6 myoblasts. *J Biol Chem* 1991; **266**: 1245–1249.

18. Nonaka I. Animal model of muscular dystrophies. *Lab Anim Sci* 1998; **48**: 8–17.
19. Sundberg C, Ivarsson M, Gerdin B, *et al.* Pericytes as collagen-producing cells in excessive dermal scarring. *Lab Invest* 1996; **74**: 452–466.
20. Laemmli UK. Cleavage of structural proteins during the assembly of the head of bacteriophage T4. *Nature* 1970; **227**: 680–685.
21. Zhao Y, Haginoya K, Iinuma K. Strong immunoreactivity of platelet-derived growth factor and its receptor at human and mouse neuromuscular junctions. *Tohoku J Exp Med* 1999; **189**: 239–244.
22. Saito A, Higuchi I, Nakagawa M, *et al.* An overexpression of fibroblast growth factor (FGF) and FGF receptor 4 in a severe clinical phenotype of fascicoscapulohumeral muscular dystrophy. *Muscle Nerve* 2000; **23**: 490–497.
23. Taylor LM, Khachigian LM. Induction of platelet-derived growth factor B-chain expression by transforming growth factor-beta involves transactivation by Smads. *J Biol Chem* 2000; **275**: 16709–16716.
24. Pinzani M, Gentilini A, Caligiuri A, *et al.* Transforming growth factor-beta 1 regulates platelet-derived growth factor receptor beta subunit in human liver fat-storing cells. *Hepatology* 1995; **21**: 232–239.
25. Ichiki Y, Smith E, LeRoy EC, *et al.* Different effects of basic fibroblast growth factor and transforming growth factor-beta on the two platelet-derived growth factor receptors' expression in scleroderma and healthy human dermal fibroblasts. *J Invest Dermatol* 1995; **104**: 124–127.
26. Schollmann C, Grugel R, Tatje D, *et al.* Basic fibroblast growth factor modulates the mitogenic potency of the platelet-derived growth factor (PDGF) isoforms by specific upregulation of the PDGF alpha receptor in vascular smooth muscle cells. *J Biol Chem* 1992; **267**: 18032–18039.
27. Eriksson A, Nister M, Leveen P, *et al.* Induction of platelet-derived growth factor alpha- and beta-receptor mRNA and protein by platelet-derived growth factor BB. *J Biol Chem* 1991; **266**: 21138–21144.
28. Walker GA, Guerrero IA, Leinwand LA. Myofibroblasts: molecular crossdressers. *Curr Top Dev Biol* 2001; **51**: 91–107.
29. Rozenlranz S, Kazlauskas A. Evidence for distinct signaling properties and biological responses induced by the PDGF receptor alpha and beta subtypes. *Growth Factors* 1999; **16**: 201–216.
30. Robertson TA, Maley MA, Grounds MD, *et al.* The role of macrophages in skeletal muscle regeneration with particular reference to chemotaxis. *Exp Cell Res* 1993; **207**: 321–331.
31. Bischoff R. Chemotaxis of skeletal muscle satellite cells. *Dev Dyn* 1997; **208**: 505–515.
32. Husmann I, Soulet L, Gautron J, *et al.* Growth factors in skeletal muscle regeneration. *Cytokine Growth Factor Rev* 1996; **7**: 249–258.
33. Yablonka-Reuveni Z, Balesteri TM, Bowen-Pope DF. Regulation of proliferation and differentiation of myoblasts derived from adult mouse skeletal muscle by specific isoforms of PDGF. *J Cell Biol* 1990; **111**: 1623–1629.
34. Gramolini AO, Wu J, Jasmin BJ. Regulation and functional significance of utrophin expression at the mammalian neuromuscular synapse. *Microsc Res Tech* 2000; **49**: 90–100.
35. Mizuno Y, Nonaka I, Hirai S, *et al.* Reciprocal expression of dystrophin and utrophin in muscles of Duchenne muscular dystrophy patients, female DMD-carriers and control subjects. *J Neurol Sci* 1993; **119**: 43–52.
36. Tinsley J, Deconinck N, Fisher R, *et al.* Expression of full-length utrophin prevents muscular dystrophy in mdx mice. *Nature Med* 1998; **4**: 1441–1444.
37. Bilak M, Askanas V, Engel KW, *et al.* Twisted tubulofilaments (TTFs) in inclusion-body myositis (IBM) muscle contain fibroblast growth factor (FGF) and its receptor (FGF-R). *Neurology* 1994; **44**: 130.
38. McLennan IS, Koishi K. Transforming growth factor-beta-2 (TGF-beta2) is associated with mature rat neuromuscular junctions. *Neurosci Lett* 1994; **177**: 151–154.
39. Toepfer M, Fischer P, Abicht A, *et al.* Localization of transforming growth factor beta in association with neuromuscular junctions in adult human muscle. *Cell Mol Neurobiol* 1999; **19**: 297–300.
40. Yoshida M, Sakuma-Mochizuki J, Abe K, *et al.* *In vivo* gene transfer of an extracellular domain of platelet-derived growth factor beta receptor by the HIV-liposome method ameliorates bleomycin-induced pulmonary fibrosis. *Biochem Biophys Res Commun* 1999; **265**: 503–508.
41. Fukutani A, Izumino K, Nakagawa Y, *et al.* Effect of the platelet-derived growth factor antagonist trapidil on mesangial cell proliferation in rats. *Nephron* 1999; **81**: 428–433.
42. Ostendorf T, Kunter U, Grone HJ, *et al.* Specific antagonism of PDGF prevents renal scarring in experimental glomerulonephritis. *J Am Soc Nephrol* 2001; **12**: 909–918.

*Epilepsia*, 44(3):366–371, 2003
Blackwell Publishing, Inc.


# Metabolic Properties of Band Heterotopia Differ from Those of Other Cortical Dysplasias: A Proton Magnetic Resonance Spectroscopy Study

*Mitsutoshi Munakata, *Kazuhiro Haginoya, §Takashi Soga, *Hiroyuki Yokoyama, *Rie Noguchi, ‡Tatsuo Nagasaka, †Takaki Murata, †Shuichi Higano, †Shoki Takahashi, and *Kazuie Iinuma

*Departments of *Pediatrics and †Diagnostic Radiology, Tohoku University School of Medicine, and ‡Division of Radiology, Tohoku University Hospital, Sendai; and §Epilepsy Hospital Bethel, Iwanuma, Japan*

**Summary:** *Purpose*: To assess the biochemical properties of band heterotopia in comparison with other cortical developmental malformations (CDMs) by using proton magnetic resonance spectroscopy ($^1$H-MRS).

*Methods*: We performed localized single-voxel $^1$H-MRS studies on 13 patients [five band heterotopia (BH), two focal cortical dysplasia (CD), two unilateral CD, one bilateral perisylvian dysplasia, three hemimegalencephaly]. CDMs other than BH were categorized as CD. Spectra were acquired from volumes of interest (VOIs) localized in the CD and in normal-appearing cortex on the contralateral side. In BH patients, the VOIs were the external cortex and the laminar heterotopia. For the BH study, spectra also were obtained from the cortex of age-matched normal volunteers.

*Results*: The spectra of CD lesions were characterized by significantly lower ratios of *N*-acetyl aspartate to creatine (NAA/Cr) and by higher choline to Cr (Cho/Cr) ratios than in the contralateral remote cortex ($p = 0.01$ and 0.01, respectively). The NAA/Cr and Cho/Cr ratios of the external cortex of BH were not significantly different from those of normal volunteers. The NAA/Cr ratio of the laminar heterotopia was not significantly different from that of the external cortex ($p = 0.12$) or normal volunteers ($p = 0.60$), whereas Cho/Cr was significantly higher in laminar heterotopias than in the external cortex ($p = 0.04$) or controls ($p = 0.03$).

*Conclusions*: $^1$H-MRS can distinguish between the metabolic properties of BH and CD. **Key Words:** Cortical dysplasia—Band heterotopia—Proton magnetic resonance spectroscopy.

Cortical developmental malformations (CDMs) are caused by disruption of neuronal proliferation, migration, or cortical organization (1,2). They are clinically important conditions, often accompanied by intractable epilepsy and neurologic developmental deficits (3,4). Band heterotopia (BH) is a CDM that is caused by disruption of neuronal migration, and it is characterized by extensive bilateral plates of heterotopic gray matter just below the normotopic cortex (5). This subcortical heterotopia has unusual functional properties that are not observed in other CDMs. Functional magnetic resonance imaging studies have shown that subcortical heterotopia is activated together with the related external cortex during a motor task, suggesting that the heterotopia may be involved in normal brain activity (6,7).

Accepted October 4, 2002.
Address correspondence and reprint requests to Dr. M. Munakata at Department of Pediatrics, Tohoku University School of Medicine, Sendai 980-8574, Japan. E-mail: muna@ped.med.tohoku.ac.jp

Neuropathologic studies have demonstrated that cytoarchitectural derangement occurs in CDMs. The characteristic abnormality in cortical dysplasia lesions is faulty cell differentiation, which produces immature, abnormal cells, such as giant neurons and bizarre glia cells, often referred to as "balloon cells" (8,9). In contrast, the abnormalities in BH are mild. The heterotopic gray matter consists of disarranged, but relatively well-differentiated, pyramidal cells (5). These distinct functional and cytoarchitectural properties that distinguish BH from other CDMs may correlate with different metabolic conditions.

Proton magnetic resonance spectroscopy ($^1$H-MRS) is a noninvasive way to evaluate metabolic conditions in tissues in vivo (10). MRS signals in the brain change in various pathologic conditions, such as metabolic diseases, brain neoplasms, epileptic foci, and CDMs (11), although BH has not been fully addressed. In this study, we used localized single-voxel $^1$H-MRS to investigate the metabolic profile of BH, and compared it with other CDMs.

## METHODS

We studied 13 patients (12 female and one male patients) with different types of CDM (Table 1). The patients' ages ranged from 1 to 34 years (average, 16 years). The objectives of this study were explained to the families and to the patients when possible, and informed consent was obtained.

The disorders were diagnosed from MR imaging (MRI) findings, with reference to a previously proposed MRI classification scheme (12). Because patients 3 and 4 were not strictly classified in the scheme, they were tentatively diagnosed as having unilateral cortical dysplasia. In both cases, the MRI showed hemispheric hypoplasia with multiple abnormal rough shallow gyri. Recently, Caraballo et al. (13) and Pascual-Castroviejo et al. (14) proved that unilateral polymicrogyria consisting of a hypoplastic hemisphere with diffuse abnormal gyri was polymicrogyria by using three-dimensional MRIs and histology. Patients 3 and 4 most likely belong to this category, although further consideration is required. Focal cortical dysplasia (CD), unilateral CD, and bilateral perisylvian dysplasia were categorized as CD and compared with BH.

Proton ($^1$H)-MRS signals are highly age dependent, especially in the first few years of life. Age-dependent changes are prominent in signals of *N*-acetyl aspartate and choline-containing compounds, whereas those of creatine and phosphocreatine are relatively stable throughout life (15). Therefore age-matched controls might be required. Because our CD patient group consisted of young children, the ethical problem of heavily sedating healthy children prevented us from making an age-matched control group. Therefore in this study, we compared the MRS signal of the lesion with that of the remote, putatively normal, contralateral cortex in the same patient by using a paired nonparametric test. By contrast, the BH patients were older, so normal healthy volunteers could be used as age-matched controls for BH. The control group consisted of five normal volunteers: three men and two women, with ages ranging from 8 to 34 years (average, 21 years).

$^1$H-MRS studies were performed at Tohoku University Hospital by using a 1.5-T MR unit that allows both imaging and spectroscopy (Magnetom Vision, Siemens). After obtaining conventional images in the axial, coronal, and sagittal planes, single-volume $^1$H spectra were obtained from a 1.5 × 1.5 × 1.5-cm voxel within CDM lesions and from the contralateral remote cortex as a control. Because of the laminar shape of the subcortical heterotopia of BH, the shape of the voxel was modified to 1.0 × 1.5 × 1.5 cm. Because peak intensity is proportional to the concentration of the substance, the change in voxel shape did not alter the signal ratios (11). Instead, the volume reduction might have reduced the signal-to-noise ratio (11), although the peaks were very recognizable in this modified voxel, as shown in Fig. 3. In the age-matched control group for BH, spectra were obtained from 1.5 × 1.5 × 1.5-cm voxels located in the parietal or occipital cortex. The repetition (TR) and echo (TE) times were 1,500 and 135 ms, respectively. After global and local shimming, and optimization of the water-suppression pulse, data were collected 128 times for each voxel and averaged.

Intense signals in the spectra were noted at 2.0, 3.0, and 3.2 ppm. The signal at 2.0 ppm is thought to be derived from *N*-acetyl–containing compounds, mainly *N*-acetyl aspartate (NAA), whereas the signal at 3.2 ppm is from choline-containing compounds (Cho), and that at 3.0 ppm is from creatine and phosphocreatine (Cr) (13). Because the Cr signal is homogeneously distributed throughout the brain and is relatively stable, even in dis-

**TABLE 1.** *Clinical features of patients with cortical developmental malformations*

| Case | Sex | Age (yr) | Category | MRI diagnosis | Seizure | | | | Mental retardation |
|---|---|---|---|---|---|---|---|---|---|
| | | | | | Onset | Type | Frequency | EEG findings | |
| 1 | F | 1 | CD | Focal CD (R;PL) | 1 yr | BTS | 0/yr | Focal sp (R;aT-mT) | – |
| 2 | F | 9 | CD | Focal CD (bilateral;FL) | 5 yr | CPS | 1/day | Diffuse HVS, focal sp (R;pF) | + |
| 3 | M | 9 | CD | Unilateral CD (R) | 4 yr | GTC | 1/day | Focal sp (R;C) | + |
| 4 | F | 15 | CD | Unilateral CD (L) | 2 yr | GTC | 1/day | Focal sp (L;F, O, R;mT) | + |
| 5 | F | 20 | CD | Bilateral perisylvian CD | 6 yr | CPS | 1/day | Focal sp (Bilat;pT, F-aT) | – |
| 6 | F | 1 | CD | Hemimegalencephaly (R) | 1 mo | SPS | 1/mo | Focal sp, sp-w (R;F, O) | + |
| 7 | F | 19 | CD | Hemimegalencephaly (R) | 18 yr | CPS | 3/wk | Focal sp, sp-w (R;O) | + |
| 8 | F | 27 | CD | Hemimegalencephaly (L) | 2 mo | CPS, GTC, MC | 5/yr | Focal sp, sp-w (L;F) | + |
| 9 | F | 9 | BH | Band heterotopia | 8 mo | CPS | 5/mo | Focal sp (L;pT-O, R;O) | + |
| 10 | F | 14 | BH | Band heterotopia | 2 yr | Multiple (Lennox)[a] | 3/day | Diffuse slow sp-w | + |
| 11 | F | 21 | BH | Band heterotopia | 4 yr | Astatic, CPS | 5/day | Focal sp, sp-w (L;C) | + |
| 12 | F | 24 | BH | Band heterotopia | 6 yr | SPS, CPS | 3/day | Focal sp (L;mT, pT, O) | + |
| 13 | F | 34 | BH | Band heterotopia | 3 mo | Multiple (Lennox)[a] | >10/day | Diffuse slow sp-w | + |

CD, cortical dysplasia (see Methods); BH, band heterotopia; R, right; L, left; PL, parietal lobe; FL, frontal lobe; BTS, brief tonic spasm; CPS, complex partial seizure; GTC, generalized tonic–clonic seizure; MS, myoclonic seizure; SPS, simple partial seizure; sp, spike; sp-w, spike and wave; HVS, high-voltage slow wave.

[a] Multiple seizure types include SPS, atypical absence, atonic, and tonic seizures.

TABLE 2. *$^1$H-MRS metabolite ratios*

| | CD (n = 8) | | BH (n = 5) | | |
|---|---|---|---|---|---|
| | Lesion | Contralateral remote cortex | Heterotopic layer | External cortex | Age-matched control (normal cortex) |
| NAA/Cr | 1.46 ± 0.37 | 2.02 ± 0.46 | 1.65 ± 0.21 | 1.72 ± 0.22 | 1.84 ± 0.09 |
| Cho/Cr | 1.14 ± 0.23 | 0.85 ± 0.14 | 0.87 ± 0.13 | 0.65 ± 0.11 | 0.60 ± 0.53 |

Values are presented as the average ± standard deviation (SD).
CD, cortical dysplasia; BH, band heterotopia; NAA/Cr, *N*-acetyl aspartate to creatine; Cho/Cr, choline to creatinine.

ease, it is often used as an internal standard (11,15). Therefore, the peak amplitudes of these three signals were measured and analyzed in terms of the NAA/Cr and Cho/Cr ratios.

The NAA/Cr and Cho/Cr ratios for CD lesions and for the contralateral side are plotted in the figures, and the summarized data are presented in Table 2 as the average ± standard deviation. Statistical differences between the CD lesions and the contralateral normal cortices were assessed by using the Wilcoxon signed-rank test, a *paired* nonparametric test. This test also was used to compare the subcortical heterotopia with the external cortex of the BH patients. Subsequently, the Mann–Whitney *U* test was used to examine the difference between the external cortex or subcortical heterotopia and the cortex of normal volunteers.

## RESULTS

Figure 1 shows a representative spectrum from CD (patient 3). Because NAA and Cho signals are age dependent (15), the $^1$H-MRS signals of the lesion were compared with those of the contralateral remote cortex in the same patient. Compared with the contralateral remote cortex (Fig. 1A), the NAA/Cr ratio was reduced in the lesion, whereas the Cho/Cr ratio was increased (Fig. 1B). The results for the eight patients with CD are plotted in Fig. 2. The NAA/Cr ratios in the CD lesions were significantly lower than those in the contralateral remote cortex (Wilcoxon signed-rank test, $p = 0.012$; Fig. 2A). In contrast, the Cho/Cr ratios in the CD lesions were significantly higher than in the contralateral remote cortex ($p = 0.012$; Fig. 2B). The average NAA/Cr and Cho/Cr ratios for the CD lesions are listed in Table 2. Patients 1 and 6 were 1-year-old children (shown by open circles in Fig. 2). The NAA/Cr ratios for the contralateral remote cortex (Fig. 2, Contra.) in these cases were lower than those in the older CD patients, whereas the Cho/Cr ratios were higher, which is in line with previously reported developmental changes in MRS signals (15). In these patients, the NAA/Cr ratios also were reduced in the CD lesion, and the Cho/Cr ratios were increased.

The NAA/Cr and Cho/Cr ratios of the external cortex of BH patients were not significantly different from those of the normal cortex of the age-matched controls (Mann–Whitney *U* test, $p = 0.12$ and 0.60, respectively). Figure 3 shows representative spectra from the external cortex and the heterotopic layer of BH (patient 11). The NAA/Cr ratios of the heterotopic layer were not significantly different from those of the external cortex (Wilcoxon signed-rank test, $p = 0.50$) or the control group cortex (Mann–Whitney *U* test, $p = 0.12$; Fig. 4A). By contrast, the Cho/Cr ratios of the laminar heterotopia

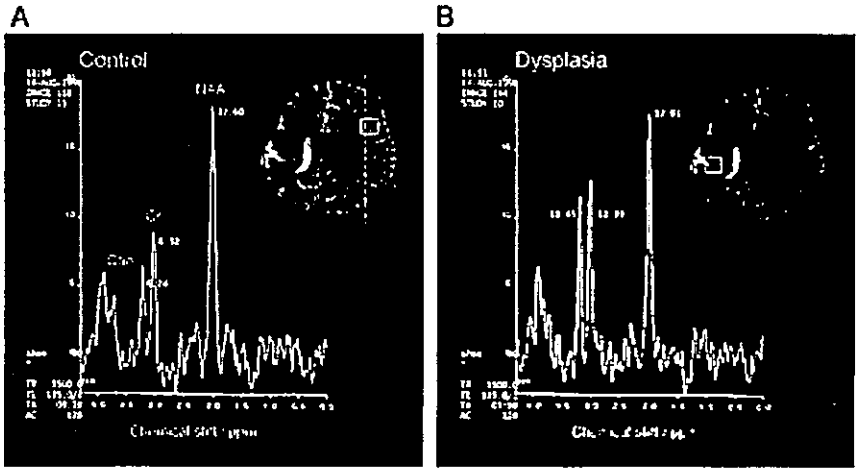


FIG. 1. $^1$H-magnetic resonance spectroscopy (MRS) spectrum acquired from a 9-year-old boy with focal cortical dysplasia. The localized volume of interest (VOI) is outlined on the magnetic resonance image (inset). Measurements were made of the remote normal cortex (A) and the dysplastic lesion (B). The resonances of choline (Cho) at 3.2 ppm, creatine (Cre) at 3 ppm, and *N*-acetyl aspartate (NAA) at 2 ppm were detected in both cases with different signal-intensity ratios.

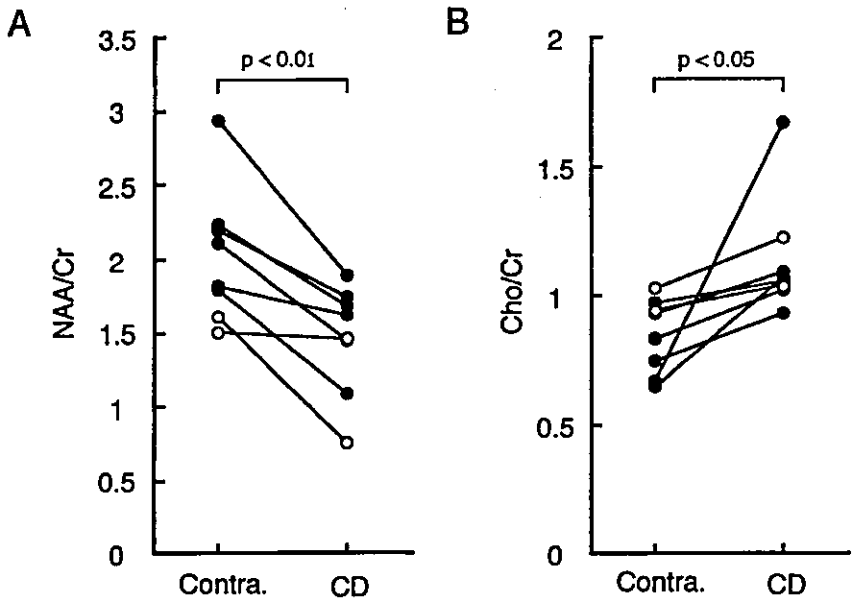


FIG. 2. The summarized $^1$H-magnetic resonance spectroscopy (MRS) results for the cortical dysplasia patients. **A:** *N*-acetyl aspartate (NAA)/creatinine (Cr) ratio in the dysplastic cortex (CD) and in the contralateral remote cortex as a control (Contra). The NAA/Cr ratio in CD was significantly lower than that in Contra ($p < 0.01$). **B:** Cho/Cr ratio in CD and in Contra. The Cho/Cr ratio was significantly elevated in CD ($p < 0.05$). Lines connect the data from the same patient. Open circles are the plots of 1-year-old patients (see text).

were significantly higher than those of the external cortex (Wilcoxon signed-rank test, $p = 0.04$) and the control group cortex (Mann–Whitney *U* test, $p = 0.03$; Fig. 4B). The average NAA/Cr and Cho/Cr ratios of the heterotopic layer, external cortex of BH, and control group cortex are summarized in Table 2.

## DISCUSSION

In this study, the NAA/Cr ratio was significantly decreased in the CD lesions, compared with the contralateral remote cortex. This result agrees with previous MRS reports concerning CD (16–18). CD lesions contain morphologically abnormal neurons, whereas the density of neurons and glia is normal (16). These neurons have unusual electrophysiologic properties (2,19). Immunocytochemically, there is a delay in the developmental switch from the $\alpha_1$ to $\alpha_2$ subunits of γ-aminobutyric acid A ($GABA_A$) receptors, and expression of the 2A (NR2A) *N*-methyl-D-aspartate (NMDA) receptor subunits also is delayed, suggesting functional immaturity of the neurons (20). These abnormalities in neuronal maturation may underlie the reduced NAA signal in the CD lesion, rather than neuronal loss or secondary gliosis.

Another significant finding in CD in our study was the increased Cho/Cr ratio in the lesions. Cho is a constituent of the phospholipid metabolism of cell membranes and may reflect membrane turnover (11). The Cho signal

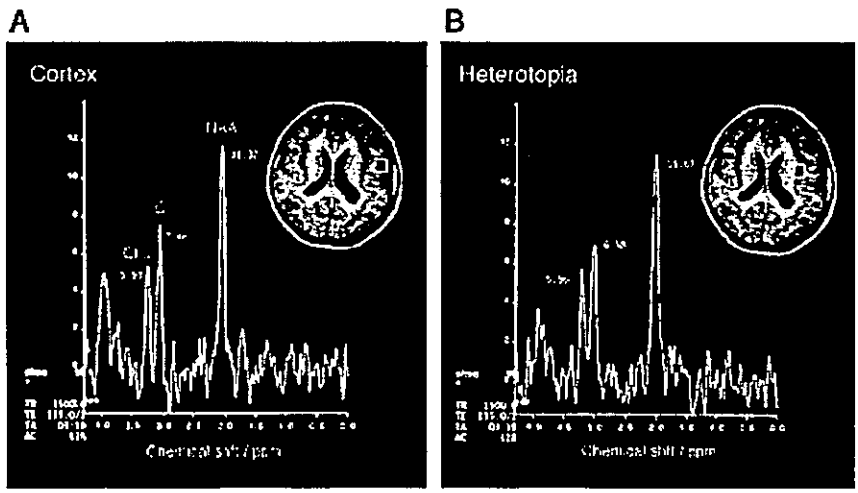


FIG. 3. $^1$H-magnetic resonance spectroscopy (MRS) spectrum acquired from a 21-year-old woman with band heterotopia. The volume of interest (VOI; inset) for the heterotopic area was modified because of its laminar structure (1.0 × 1.5 × 1.5 cm). Measurements of the external control cortex **(A)** and laminar heterotopia **(B)** were made.